

---

# Site U1377<sup>1</sup>

---

Expedition 330 Scientists<sup>2</sup>

## Chapter contents

Background and objectives	1
Operations	2
Sedimentology	3
Paleontology	5
Igneous petrology and volcanology	7
Alteration petrology	9
Structural geology	11
Geochemistry	12
Physical properties	13
Paleomagnetism	15
Microbiology	16
References	17
Figures	19
Tables	52

## Background and objectives

Site U1377 (prospectus Site LOUI-4B) on Hadar Guyot (168.6°W Guyot) was the sixth and final site completed during Integrated Ocean Drilling Program (IODP) Expedition 330 (Fig. F1). Hadar Guyot, the youngest seamount targeted during Expedition 330, has a measured <sup>40</sup>Ar/<sup>39</sup>Ar age of 50.1 Ma (Koppers et al., 2011), similar to that of Koko Seamount in the Hawaiian-Emperor Seamount Trail. Hadar Guyot shows no evidence of tilting and, together with another small guyot (located northeast at 168.3°W) and one of the largest guyots (located southeast at 168.0°W), forms a cluster of seamounts in the Louisville Seamount Trail that formed on top of the Wishbone Scarp (Fig. F1). Hadar Guyot is the smallest seamount cored during Expedition 330, consisting of a single volcanic center with a base diameter of ~25 km. Like all Louisville Seamounts drilled, it has a flat summit plain, defining it as a guyot that at some point must have emerged above sea level as a volcanic island. Site U1377 was placed near the middle of this small edifice (Fig. F2), away from its shelf edges and any packages of dipping volcanoclastics on its flanks. The approach is similar to that used for Sites U1375 and U1376, but contrary to that used for Sites U1372, U1373, and U1374, which targeted in particular volcanoclastic rocks from the flank sequences. Side-scan sonar reflectivity and 3.5 kHz subbottom profiling data indicate that Site U1377 is covered with <8 m of pelagic sediment, and seismic reflection profiles suggest that this site is characterized by a 52 m thick section of dipping volcanoclastics overlying igneous basement.

The original drilling plan was to recover soft sediment using a gravity-push approach with little or no rotation of the rotary core barrel assembly, followed by standard coring into the volcanoclastic material and 350 m into igneous basement. A full downhole logging series was planned, including the standard triple combination and Formation MicroScanner-sonic tool strings, the Ultrasonic Borehole Imager tool, and the third-party Göttingen Borehole Magnetometer tool. Like at Site U1375 on Acheron Guyot, drilling at Site U1377 became difficult after instabilities were met in the uppermost part of the seamount formation, likely from the presence of loose clast-rich volcanic breccia in the sediment cover, which was only sparsely recovered (16% and 39% recovery in Holes U1377A and U1377B, respectively). Drilling reached 53.3 meters below seafloor (mbsf) in Hole U1377A and 37.0 mbsf in

<sup>1</sup>Expedition 330 Scientists, 2012. Site U1377. In Koppers, A.A.P., Yamazaki, T., Geldmacher, J., and the Expedition 330 Scientists, *Proc. IODP, 330*: Tokyo (Integrated Ocean Drilling Program Management International, Inc.). doi:10.2204/iodp.proc.330.108.2012

<sup>2</sup>Expedition 330 Scientists' addresses.



Hole U1377B, but because of time constraints and shallow penetration no logging was carried out.

## Objectives

Drilling during Ocean Drilling Program (ODP) Leg 197 provided compelling evidence for the motion of mantle plumes by documenting a large  $\sim 15^\circ$  shift in paleolatitude for the Hawaiian hotspot (Tarduno et al., 2003; Duncan et al., 2006). This evidence led to testing two geodynamic end-member models during Expedition 330, namely that the Louisville and Hawaiian hotspots moved coherently over geological time (Courtilot et al., 2003; Wessel and Kroenke, 1997) or, quite the opposite, that these hotspots show considerable interhotspot motion, as predicted by mantle flow models (Steinberger, 2002; Steinberger et al., 2004; Koppers et al., 2004; Steinberger and Antretter, 2006; Steinberger and Calderwood, 2006). The most important objective of Expedition 330, therefore, was to core deep into the igneous basement of four seamounts in the Louisville Seamount Trail in order to sample a large number of in situ lava flows ranging in age between 80 and 50 Ma. With a sufficiently large number of these independent cooling units, high-quality estimates of their paleolatitude can be determined and any paleolatitude shift (or lack thereof) can be compared with that defined by seamounts in the Hawaiian-Emperor Seamount Trail. For this reason, Expedition 330 mimicked the drilling strategy of Leg 197 by drilling seamounts equivalent in age to Detroit (76–81 Ma), Suiko (61 Ma), Nintoku (56 Ma), and Koko (49 Ma) Seamounts in the Emperor Seamount Trail. Accurate paleomagnetic inclination data are required for the drilled seamounts in order to establish a record of past Louisville hotspot motion, and, together with high-resolution  $^{40}\text{Ar}/^{39}\text{Ar}$  age dating of the cored lava flows, these data will help us constrain the paleolatitudes of the Louisville hotspot between 80 and 50 Ma. Such comparisons are of fundamental importance in determining whether these two primary hotspots have moved coherently or not and in understanding the nature of hotspots and convection in the Earth's mantle.

Expedition 330 also aimed to provide important insights into the magmatic evolution and melting processes that produced and constructed Louisville volcanoes as they progressed from shield to postshield, and perhaps posterosional, volcanic stages. Existing data from dredged lava suggest that the mantle source of the Louisville hotspot has been remarkably homogeneous for as long as 80 m.y. (Cheng et al., 1987; Hawkins et al., 1987; Vanderkluyesen et al., 2007; Beier et al., 2011). However, because Site

U1377 is located in close proximity to the Wishbone Scarp (Fig. F1), there was speculation that the recovered rocks might have a slightly different geochemical composition as a result of a possible step in lithosphere thickness across the scarp (Beier et al., 2011). In addition, all dredged basalt is predominantly alkalic and possibly represents a mostly alkalic shield-building stage, in contrast to the tholeiitic shield-building stage of volcanoes in the Hawaiian-Emperor Seamount Trail (Hawkins et al., 1987; Vanderkluyesen et al., 2007; Beier et al., 2011). Therefore, the successions of lava flows cored during Expedition 330 will help us characterize the Louisville Seamount Trail as the product of a primary hotspot and test the long-lived homogeneous geochemical character of its mantle source. Analyses of melt inclusions, volcanic glass samples, high-Mg olivine, and clinopyroxene phenocrysts will provide further constraints on the putative homogeneity of the Louisville plume, its compositional evolution between 80 and 50 Ma, its potential temperatures, and its associated magma genesis, volatile outgassing, and magmatic differentiation. Incremental heating  $^{40}\text{Ar}/^{39}\text{Ar}$  age dating will allow us to establish age histories within each drill core, delineating any transitions from the shield-building phase to the postshield capping and posterosional stages.

Finally, basalt and sediment cored at Site U1377 were planned for use in a range of secondary objectives, such as searching for active microbial life in the old seamount basement and determining whether fossil traces of these microbes were left behind in volcanic glass or on rock biofilms. We also planned to determine  $^3\text{He}/^4\text{He}$  and  $^{186}\text{Os}/^{187}\text{Os}$  signatures of the Louisville mantle plume to evaluate its potential deep-mantle origin, to use oxygen and strontium isotope measurements on carbonates and zeolites in order to assess the magnitude of carbonate vein formation in aging seamounts and its role as a global  $\text{CO}_2$  sink, to age date celadonite or other alteration minerals for estimating the total duration of low-temperature alteration following seamount emplacement, and to determine the hydrogeological and seismological character of the seamount basement.

## Operations

The 392 nmi transit to Site U1377 was made without incident at an average speed of 11.2 kt. By 0930 h on 5 February 2011 the vessel was positioning on the coordinates of Hole U1377A (all times are New Zealand Daylight Time, Universal Time Coordinated [UTC] + 13 h). The vibration-isolated television (VIT) frame was launched after a three-stand rotary core

barrel drilling assembly was made up with a new Type C-4 bit and a refurbished mechanical bit release and deployed to 988 meters below rig floor (mbrf).

Tagging of the seafloor at 1262.0 mbrf (1250.8 meters below sea level [mbsl]) was observed at 1435 h. The seabed appeared to be covered mostly by a fine layer of sediment and a few scattered rocks (Table T1). After the VIT frame was recovered and the top drive was picked up, Hole U1377A was spudded at 1510 h. Rotary coring advanced amid increasingly difficult hole conditions and overall poor recovery. Finally, after coring to a depth of 53.3 mbsf, the hole became too unstable and had to be abandoned. The bit cleared the seafloor at 1815 h on 6 February and was picked up to 1103 mbrf. Average recovery for Hole U1377A was 16.4%. The time expended on Hole U1377A was 12.5 h.

It was decided to offset the vessel ~500 m south of Hole U1377A and attempt to spud another hole at this site. The vessel was positioned after a 30 min offset with the bit 159 m above the seafloor. The VIT frame was deployed and showed a seafloor covered with soft sediment. The driller tagged the seafloor at 1250.8 mbsl. Hole U1377B was spudded at 2325 h on 6 February, and rotary coring advanced to 18.1 mbsf. During the retrieval of the core barrel for Core 330-U1377B-2R, unstable parts of the formation fell into the hole and were subsequently recovered in the core barrel of Core 330-U1377B-3G. Because the recovered material cannot be assigned to a specific depth, this core was curated as a “ghost” core, as indicated by the suffix “G” in the core name. Below 18.1 mbsf the formation was stable enough to allow drilling to advance to a final depth of 37.0 mbsf, when the allocated time on site expired. As the last core barrel was being retrieved, the coring line was coated with a rust inhibitor in accordance with routine. After the drill string and beacon were recovered and the rig floor was secured for transit, the vessel departed Site U1377 for Auckland, New Zealand, at 0730 h on 8 February. The time on Hole U1377B was 57.5 h, and the total time on site was 70.0 h (2.9 days). Because of concerns of moderate headwinds and rough seas on the transit to Auckland, the vessel departed approximately 18 h earlier than originally planned.

## Sedimentology

Sediment at Site U1377 was encountered in the sedimentary cover of Hadar Guyot. Two stratigraphic units were defined on the basis of compositional and textural characteristics of the sediment at macroscopic and microscopic scales in Holes U1377A and U1377B (Fig. F3).

## Hole U1377A

Although the exact nature and thickness of the units are poorly constrained because of very low (<1%) recovery, two stratigraphic units were defined in Hole U1377A, and these likely correspond to Units I and II defined in Hole U1377B (see below):

- Unit I (poorly constrained interval extending from 0 to at least 0.03 mbsf): pelagic cap of drilled seamount. The lithology of this unit was defined on the basis of sediment from the core catcher of Core 330-U1377A-1R and consists of light gray nannofossil foraminiferal ooze.
- Unit II (poorly constrained interval extending from 6.10 to at least 6.24 mbsf): the lithology of this unit is defined on the basis of sediment from the core catcher of Core 330-U1377A-2R and consists of bioturbated foraminiferal limestone with ferromanganese encrustations.

### Unit I

Interval: 330-U1377A-1R-1, 0–3 cm

Depth: 0–0.03 mbsf

Age: early Pliocene to Holocene

Stratigraphic Unit I corresponds to the sediment retrieved in the core catcher of Core 330-U1377A-1R. Its exact extension is poorly constrained because of very low (<1%) core recovery in the uppermost part of Hole U1377A (Fig. F3). The lower boundary of this unit was not sampled. The sediment of Unit I is composed of light gray nannofossil foraminiferal ooze with volcanic glass fragments. Foraminiferal and nannofossil assemblages define an early Pliocene to Holocene age of deposition (see “Paleontology”).

Smear slide observations (Sample 330-U1377A-1R-CC-PAL-SED, 0–2 cm) showed that the nannofossil foraminiferal ooze includes some fragments of fresh volcanic glass and plagioclase.

### Unit II

Interval: 330-U1377A-2R-1, 0–14 cm

Depth: 6.10–6.24 mbsf

Age: between middle and late Eocene

Stratigraphic Unit II corresponds to the sediment retrieved in the core catcher of Core 330-U1377A-2R, and its lower boundary was not recovered (Fig. F3). Unit II includes bioturbated multicolor foraminiferal limestone with ferromanganese encrustations and black dendrites (Fig. F4A). Foraminiferal assemblages found in the limestone provide an age of deposition between the middle and late Eocene (see “Paleontology”). X-ray fluorescence analyses using the shipboard Thermo Scientific Niton XL3 Analyzer (see XL3\_EVAL.PDF in XRF in “Supplementary mate-

rial”) show that the limestone has a high phosphorous content. These analyses also confirm the occurrence of ferromanganese material in most of the limestone.

Some cuttings accumulated in the core catcher during retrieval of Core 330-U1377A-3R, including some sand-size grains of white and yellowish foraminiferal limestone and possible echinoderm fragments. These fragments originated from the interval above 24.50 mbsf (the bottom depth of the cored interval for this core) and likely indicate the presence of unrecovered shallow-water or hemipelagic limestone in Unit II above.

Thin section observations (Sample 330-U1377A-2R-1, 15–17 cm [Thin Section 269]) showed that limestone recovered in Unit II includes very abundant planktonic foraminifers with rare echinoderm fragments and altered rounded glass fragments. The dendroid shapes of probable ferromanganese-oxide minerals were often observed in thin section.

### Hole U1377B

Although recovery of the uppermost sequence in Hole U1377B was very poor, two stratigraphic units were defined, and these likely correlate with Units I and II in Hole U1377A:

- Unit I (poorly constrained interval from 0 to at least 0.79 mbsf): pelagic cap of drilled seamount composed of pale yellowish nannofossil foraminiferal ooze.
- Unit II (poorly constrained interval from 0.79 to 1.08 mbsf): older sedimentary cover of drilled seamount. This unit includes multicolor basalt conglomerate with ferromanganese encrustations (Section 330-U1377B-1R-2), as well as bioturbated foraminiferal limestone with ferromanganese encrustations and foraminiferal limestone with basalt clasts encountered as dropped pieces in ghost Core 330-U1377B-3G (see below).

#### Unit I

Interval: 330-U1377B-1R-1, 0–79 cm

Depth: 0–0.79 mbsf

Age: early Pliocene to Holocene

Because of poor recovery in Hole U1377B, Unit I is poorly constrained, extending from the seafloor to at least 0.79 mbsf (Fig. F3). Although it was possibly sampled in underlying Section 330-U1377B-1R-2 or ghost Core 330-U1377B-3G (see below), the lower boundary of Unit I was not identified. Macroscopic and smear slide (Sample 330-U1377B-1R-1-SED, 10 cm) observations revealed that Unit I is composed of pale yellow nannofossil foraminiferal ooze with rare volcanic glass fragments (Fig. F4B). Foraminiferal

and nannofossil assemblages define a Pliocene to Holocene age of deposition (see “Paleontology”).

#### Unit II

Interval: 330-U1377B-1R-2, 0–29 cm

Depth: 0.79–1.08 mbsf

Age: between late Paleocene and early Eocene

Stratigraphic Unit II corresponds to a 0.29 m thick sedimentary unit, the exact interval of which is poorly constrained because of low recovery in Hole U1377B (Fig. F3). Unit II includes poorly sorted multicolor basalt conglomerate with ferromanganese encrustations (Fig. F4C). The clasts in the conglomerate range in size from coarse sand to boulder. The largest clasts are rounded, whereas the smallest clasts are generally angular. The conglomerate is heterolithic and includes distinct types of basalt clasts (see “Igneous petrology and volcanology”), as well as few clasts of volcanic sandstone-breccia and shallow-marine bioclasts (echinoderms, larger foraminifers, bryozoans, red algae, and shell fragments). The matrix of the conglomerate is composed of bioturbated multicolor foraminiferal limestone with ferromanganese encrustations. A geopetal structure defined by infilling of foraminiferal limestone in a cavity or burrow occurs in Section 330-U1377B-1R-2, 5.5 cm (Point 2 in Fig. F4C). Foraminiferal assemblages found in the matrix of the conglomerate provide an age of deposition between the late Paleocene and early Eocene (see “Paleontology”).

Partial collapse of the hole during drilling led to the retrieval of a ghost core (Core 330-U1377B-3G; see “Operations”) that contains rock fragments fallen from the previously penetrated interval between the seafloor and 18.10 mbsf. Five pieces of sediment were found in the ghost core (Fig. F4D). Four pieces are composed of foraminiferal limestone with ferromanganese encrustations that closely resembles the limestone of Unit II in Hole U1377A. Another piece of sediment (Piece 7) contains the following lithologies (from top to bottom):

- Bioturbated foraminiferal limestone with rare shallow-marine bioclasts and sand-size altered glass fragments (Point 3 in Fig. F4D); this limestone is similar to that sampled in Hole U1377A (Unit II);
- Ferromanganese crust with concentric layering (Point 2 in Fig. F4D); and
- Grayish foraminiferal limestone with several types of basalt clasts (see “Igneous petrology and volcanology”), a small gastropod with geopetal structure, echinoderm fragments, shell fragments, and larger benthic foraminifers (Point 1 in Fig. F4D); this limestone closely resembles the grayish

limestone found in the basalt conglomerate in the upper part of Hole U1377B (Section 330-U1377B-1R-2).

The orientation of this piece is well constrained by a geopetal structure found in a gastropod and by the texture of the ferromanganese crust. This piece is therefore believed to provide reliable indications on the stratigraphic arrangement of the distinct types of sediment found at Site U1377 (see below).

Thin section observations (Sample 330-U1377B-1R-2, 8–12 cm [Thin Section 276]) showed that the limestone recovered in Unit II is a poorly washed grainstone with very abundant planktonic foraminifers and rare larger benthic foraminifers, echinoderm fragments, altered rounded glass fragments, plagioclase, and fish debris.

### Interpretation of sediment at Site U1377

Although characterization of the stratigraphy at Site U1377 was limited by very poor recovery, observations in Holes U1377A and U1377B allowed definition of a consistent sedimentary pattern on top of Hadar Guyot. The uppermost sediment (Unit I) recovered in both holes is composed of early Pliocene to Holocene nannofossil foraminiferal ooze (see “[Paleontology](#)”) that strongly resembles the soft sediment recovered in the uppermost part of Site U1372 on Canopus Guyot, Site U1374 on Rigil Guyot, and Site U1375 on Achernar Guyot. Similar to preceding sites, the soft sediment recovered at Site U1377 on Hadar Guyot is considered to reflect recent pelagic sedimentation on top of the drilled seamount. Cores and cuttings retrieved in Holes U1377A and U1377B support the existence of a lithologically consistent Unit II at Site U1377. Two distinct lithofacies and several ferromanganese encrustations were recognized in this unit, which indicates that the sediment represents one or more condensed sections on top of Hadar Guyot. Lithofacies 1 of Unit II corresponds to bioturbated foraminiferal limestone with ferromanganese encrustations and rare shallow-marine bioclasts (see “[Paleontology](#)”). This lithofacies occurs in Section 330-U1377A-2R-1 and ghost Core 330-U1377B-3G (Fig. [F4](#)) and is interpreted to reflect sedimentation in a pelagic to hemipelagic environment on the basis of highly abundant planktonic foraminifers and few shallow-water bioclasts. Lithofacies 2 of Unit II corresponds to heterolithic basalt conglomerate with a matrix composed of foraminiferal limestone with shallow-marine bioclasts (see “[Paleontology](#)”). This lithofacies is also associated with ferromanganese encrustations and occurs in Section 330-U1377B-1R-2, ghost Core 330-U1377B-3G (Fig. [F4](#)), and cuttings in the core catcher of Core 330-U1377A-3R. Lithofacies 2 is

interpreted to reflect deposition in a possible shallow-marine to hemipelagic environment on the basis of its abundance of planktonic foraminifers with well-preserved shallow-marine macrofossils and rounded basalt pebbles. Very low recovery at Site U1377 did not allow a determination of the exact thickness and recurrence of these two lithofacies. However, an unoriented limestone piece in ghost Core 330-U1377A-3G (Piece 7) includes (from bottom to top) Lithofacies 2, a ferromanganese crust, and Lithofacies 1 (Fig. [F4](#)). The sedimentary texture of this piece and the paleontological ages of Lithofacies 1 and 2 (between middle and late Eocene and between late Paleocene and early Eocene, respectively; see “[Paleontology](#)”) suggest that deposition of Lithofacies 2 occurred prior to Lithofacies 1. Possibly, this may reflect transition from a shallow-marine to hemipelagic-pelagic environment of deposition on Hadar Guyot between the late Paleocene and late Eocene.

## Paleontology

Nannofossil foraminiferal ooze (Unit I), along with foraminiferal limestone and basaltic conglomerate (Unit II), were recovered from both Holes U1377A and U1377B on Hadar Guyot. In Hole U1377A, 6.1 m of advancement with Core 330-U1377A-1R retrieved <25 cm<sup>3</sup> of the ooze, and 9.0 m of advancement with Core 2R recovered a 14 cm long section of the conglomerate of Unit II. In Hole U1377B, 9.1 m of sediment and sedimentary rock were presumed to have been penetrated with Core 330-U1377B-1R, but only 0.79 m of the ooze and 0.29 m of the conglomerate were recovered. The soft sediment of both holes is thought to have been mechanically disturbed during drilling and reworked by flushing of sediment within the core liner during retrieval. Consequently, it is assumed that a mixture of individual sequences within Unit I were recovered from Sections 330-U1377A-1R-CC and 330-U1377B-1R-1 and 1R-2. Although Units I and II show similar lithologies in Holes U1377A and U1377B, precise stratigraphic correlation of Units I and II between the two holes could not be accomplished because of very low recovery rates.

### Calcareous nannofossils

The nannofossil foraminiferal ooze of Unit I recovered in Section 330-U1377A-1R-CC is composed of a mixture of yellowish-brown nannofossil ooze and white winnowed foraminiferal ooze. The winnowed foraminiferal ooze mainly consists of planktonic foraminifers with only a small percentage of fine facies. The nannofossil foraminiferal ooze contains a

higher percentage of fine fraction compared to the winnowed foraminiferal ooze and to samples at all previous sites (U1372–U1376). The Unit I ooze recovered in Sections 330-U1377B-1R-1 and 1R-2 consists of pale yellow winnowed nannofossil foraminiferal ooze with a small amount fine fraction. Section 1R-2 is composed of limestone and basaltic conglomerate, but the core catcher of Core 1R contained washed foraminiferal ooze that was used for nannofossil and microfossil analyses. The pelagic ooze recovered from both Holes U1377A and U1377B indicates a preliminary age of mid-Pleistocene–Holocene (Fig. F5; Tables T2, T3, T4).

### Hole U1377A

Two samples from Hole U1377A at Hadar Guyot were analyzed for calcareous nannofossil content. Core 330-U1377A-1R is estimated to have penetrated 6 m and has an assemblage dominated by small *Gephyrocapsa* but also contains *G. caribbeanica* and *G. oceanica*. Neogene background species *Helicosphaera kamptneri* and *Calcidiscus leptoporus* were frequently observed. Specimens of *Reticulofenestra pseudoumbilica* were seen along with late Pliocene *Discoaster* species, but they are few. On the basis of the dominant abundance of *Gephyrocapsa* and Pleistocene species, this sample is preliminarily assigned to Zones CN13–CN15 (mid-Pleistocene to Holocene).

The second sample from the core catcher of Core 330-U1377A-1R was tan nannofossil foraminiferal ooze with a higher percentage of fine fraction containing a virtually identical assemblage to that of the first sample. The only immediately observed difference between the two samples was the frequent occurrence of *Ceratolithus cristatus* in the assemblage of the tan sediment. It, too, is preliminarily assigned to Zones CN13–CN15 (mid-Pleistocene to Holocene).

### Hole U1377B

The white winnowed nannofossil foraminiferal ooze sampled in Hole U1377B, as retrieved from the core catcher of Core 330-U1377B-1R, appears visually identical to the white foraminiferal ooze of Section 330-U1377A-1R-CC and also has a nearly identical nannofossil assemblage. One abundant specimen of *Amaurolithus primus* (Zones CN9b–CN11; late Miocene–early Pliocene) was found, but its presence is thought to result from disturbance during coring. The age of this sample is also given a preliminary assignment of Zones CN13–CN15 (mid-Pleistocene to Holocene).

### Planktonic foraminifers

Unit I in both Holes U1377A and U1377B provided sufficient samples to study the planktonic foraminifers. In addition, thin sections made from Unit II

rocks allowed successful identification of planktonic foraminifers of the limestone and basaltic conglomerate in Unit II. Planktonic foraminiferal faunas found in the thin sections made from Samples 330-U1377A-2R-1, 15–17 cm (6.25 mbsf), and 330-U1377B-1R-2, 8–12 cm (0.87 mbsf), indicate preliminary ages between middle and late Eocene and between late Paleocene and early Eocene, respectively (Fig. F5; Table T5).

### Hole U1377A

One sample from Unit I, one from Unit II, and two from the igneous rocks in Unit III, were analyzed for planktonic foraminiferal biostratigraphy. Sample 330-U1377A-1R-CC (0.0 mbsf) of Unit I is composed of sandy foraminiferal ooze containing *Globigerina bulloides*, *Globorotalia (Globoconella) inflata*, *Globorotalia (Truncorotalia) crassaformis*, and *Orbulina universa*. More than 50% of washed grains are composed of planktonic foraminifers showing well-preserved whitish tests. In addition to these major species, *Globigerinoides extremus*, *Globorotalia (Truncorotalia) truncatulinoides*, and *Sphaeroidinellopsis seminulina* (indicative of older than early Pleistocene, younger than early Pleistocene, and older than early Pliocene, respectively) were observed in this sample. The stratigraphic ranges of these species do not overlap, which implies that the specimens were reworked from different stratigraphic positions because of drilling disturbance. The preliminary age of this sample is assigned to early Pliocene–Holocene (Fig. F5; Table T3).

A thin section of Unit II foraminiferal limestone from Sample 330-U1377A-2R-1, 15–17 cm (6.25 mbsf), contains *Acarinina* sp., *Globigerinatheka* sp., and *Subbotina* spp. (Fig. F6). The test material of these individuals is relatively well preserved. In fact, the pore structure and layering of tests are clearly visible in the section surface (Fig. F6). The stratigraphic range of genus *Globigerinatheka* indicates that this sample is preliminarily correlated to planktonic foraminiferal Zones E8–E16 (middle–late Eocene) (Fig. F5; Table T5).

Although Unit III is composed of basaltic basement, rock cuttings recovered from Sample 330-U1377A-3R-1, 116–121 cm (16.26 mbsf), contain echinoderm fragments with no planktonic foraminifers, indicative of a relatively shallow marine environment. Therefore, though not recovered, a shallow-marine or hemipelagic sequence should be present between the Unit I nannofossil foraminiferal ooze and the Unit III basalt.

### Hole U1377B

Unconsolidated foraminiferal ooze of Unit I and cuttings from the cores drilled into the consolidated se-

quence of trachybasalt (Unit III) were sampled for planktonic foraminiferal biostratigraphy. Although Unit II (Section 330-U1377B-1R-2) is composed of foraminiferal limestone and basaltic conglomerate, a small amount of washed sandy foraminiferal ooze (likely derived from Unit I) was recovered at 28–29 cm in Section 1R-2 (10.7 mbsf). This sample contains *Gr. (G.) inflata*, *Gr. (T.) crassaformis*, and *Gr. (T.) truncatulinooides*. More than 50% of the washed-down sand-size grains are composed of planktonic foraminifers. The occurrence of these species indicates a preliminary age of middle Pleistocene–Holocene. Nonetheless, *Gs. extremus* and *Ss. Seminulina* (indicative of older than early Pleistocene and older than early Pliocene, respectively) co-occur in this sample. As was observed in Hole U1377A, this sample also encloses reworked individuals from various other horizons. The preliminary age of this sample was assigned to early Pliocene–Holocene (Fig. F5; Table T4). Cuttings from Sample 2R-3, 20–40 cm (12.20 mbsf), contain no biogenic fragments.

A thin section of Unit II consolidated limestone from Sample 330-U1377B-1R-2, 8–12 cm (0.89 mbsf), contains *Acarinina* sp., *Morozovella* sp. (*Morozovella* cf. *acuta*?), *Subbotina* spp., and a few echinoderm fragments (Fig. F7). Although precise species identification needs to be refined postexpedition, on the basis of the occurrence of *M. cf. acuta* this sample could be correlated to Zones P4b–E2 (late Paleocene–early Eocene) (Fig. F5; Table T5).

### Preliminary age estimation for Site U1377

Both nannofossil and planktonic foraminiferal faunas recovered from Unit I ooze are composed of a mixture of Holocene, Pleistocene, and Pliocene species because of drilling disturbance. Although the mixed nature of these microfossil faunas and the low recovery rate prevent stratigraphic correlation of Unit I between Holes U1377A and U1377B, the preliminary age of Unit I in both holes is assigned to the early Pliocene–Holocene. A partly older age of this unit may, however, be indicated by the occurrence of a specimen of *Amaurolithus primus* (late Miocene–early Pliocene) in Section 330-U1377A-1R-CC.

A thin section made from Unit II in Hole U1377A contains predominantly planktonic foraminifers, whereas one from Hole U1377B contains not only planktonic foraminifers but also larger benthic foraminifers and macrofossils. This indicates that the depositional depth of Unit II recovered in Hole U1377B was shallower than that recovered in Hole U1377A, which is in agreement with the interpretation that distinct levels of Unit II were recovered in each hole (see “Sedimentology”). The planktonic foraminiferal genus *Globigerinatheka* found in Sample 330-

U1377A-2R-1, 15–17 cm, evolved during the middle Eocene and went extinct at the end of the Eocene (Pearson et al., 2006). Although precise species identification was not made on board, this generic range indicates a preliminary age between middle and late Eocene for Unit II of Hole U1377A. On the other hand, *Morozovella* sp. (*Morozovella* cf. *acuta*?) found in Unit II of Hole U1377B has a biostratigraphic range of Zones P4b–E2 (Pearson et al., 2006), indicative of between the late Paleocene and early Eocene, which is slightly older than the age of Unit II in Hole U1377A. Although the low recovery rate of Unit II in both holes prevents precise stratigraphic correlation, the age discrepancy between the Unit II limestone in Hole U1377A and that in Hole U1377B implies that either distinct layers of Unit II were sampled in each hole or a few diachronous limestone horizons were developed on Hadar Guyot. The former is more likely, as indicated by lithostratigraphic relationships based on observation of ghost Core 330-U1377B-3G (see “Sedimentology”) and the close proximity of the holes. Although the low recovery rate prevents precise stratigraphic constraint, a ~30 m.y. unconformity may exist between Units I and II.

## Igneous petrology and volcanology

Two holes were drilled at Site U1377 on Hadar Guyot. In Holes U1377A and U1377B, 38.2 and 27.9 m of igneous rocks were penetrated after igneous basement was reached at 15.1 and 9.1 mbsf, respectively. The igneous sequence was divided into six lithologic units in Hole U1377A and 18 lithologic units in Hole U1377B. In both holes these units were grouped into a single stratigraphic unit (Unit III in each case; Fig. F8). To help achieve the paleomagnetic objectives of this expedition, each of the igneous lithologic units was assigned an in situ confidence index (ISCI) following the procedures described in “Igneous petrology and volcanology” in the “Methods” chapter (Expedition 330 Scientists, 2012a). The lithologic units and their ISCI values are summarized in Table T6. In this section we describe the igneous units in Hole U1377A and then the volcanic components in the sedimentary units of Hole U1377B, followed by each of the igneous units in Hole U1377B. Our interpretation of the entire igneous succession follows.

### Hole U1377A

#### Lithologic and stratigraphic igneous units

##### Unit III

Interval: Sections 330-U1377A-3R-1, 0 cm, to 6R-3, 118 cm

Depth: 15.10–47.46 mbsf

Lithology: banded aphyric to highly olivine-phyric trachybasalt

Lithologic units: 1–6

The six lithologic units defined in Hole U1377A are dominantly aphyric lava flows with occasional olivine-phyric intervals. These lithologic units were combined to form stratigraphic Unit III. Strong flow banding, defined by variation in grain size and vesicle abundance, occurs throughout Unit III (Fig. F9), and in some intervals it causes the rocks to split into parallel-sided fragments (e.g., Fig. F9B). Strong flow banding is a common feature of intermediate alkaline volcanic rocks, and the intermediate composition of Unit III is confirmed by the only shipboard chemical analysis carried out on a rock sample from Site U1377 (Sample 330-U1377A-3R-2, 2–4 cm). Because this sample contains 55 wt% SiO<sub>2</sub> and 3 wt% MgO (see “[Geochemistry](#)”) despite being moderately olivine-phyric, we applied the name “trachybasalt” to all igneous units from Hole U1377A (and also Hole U1377B). Postcruise chemical analysis will allow more rigorous identification of the igneous rock types.

Lithologic Unit 1 is 1.48 m thick and is composed of aphyric trachybasalt with vesicle bands that run vertically through the core. Its upper contact with the sedimentary cover (stratigraphic Units I and II; see “[Sedimentology](#)”) and its lower contact with lithologic Unit 2 were not recovered. Lithologic Unit 2 is a 0.17 m thick interval of moderately olivine-phyric trachybasalt from which the sample providing the trachybasalt composition was taken (see “[Geochemistry](#)”). The lower boundary of Unit 2 was not recovered. Lithologic Unit 3 was inferred to make up the bulk (20.36 m) of the igneous succession recovered from Hole U1377A, although we cannot be certain of this because of low core recovery (28%). Unit 3 is composed of aphyric trachybasalt, except for two thin intervals that contain altered olivine phenocrysts. One of these intervals is 13 cm thick and highly olivine-phyric, and the other is 15 cm thick and moderately olivine-phyric. Centimeter- to sub-centimeter-scale flow banding occurs throughout the unit. Grain size varies from aphanitic to fine grained, and vesicle abundance ranges from 0% to 25% between adjacent layers (Fig. F9A, F9B). Lithologic Unit 4 is distinct from Unit 3 in being sparsely olivine-phyric. Only 35 cm was recovered, and this includes neither the upper nor the lower contact. The 1.99 m thick lithologic Unit 5 is visually distinctive in its abundance (20%) of vesicles. It is moderately olivine-phyric and also contains 0.5% augite phenocrysts. Lithologic Unit 6 makes up the lower

26 cm of Hole U1377A and consists of poorly recovered aphyric trachybasalt rubble.

## Hole U1377B

### Basaltic clasts in sedimentary Unit II

Two types of basalt clasts were observed in the conglomerate of stratigraphic Unit II in Hole U1377B (see “[Sedimentology](#)”) on the basis of the appearance of the larger clasts in hand specimen. Both types differ in appearance from the trachybasalt of Unit III:

- Type 1: highly olivine-phyric basalt that is brown-orange, with 10% olivine phenocrysts (altered; maximum size = 5 mm, modal size = 2 mm) and 2% augite phenocrysts (maximum size = 4 mm, modal size = 2 mm). The groundmass is fine grained, with no vesicles.
- Type 2: aphyric basalt that is brown-gray and contains no phenocrysts. The groundmass is fine grained, with 1% vesicles (low sphericity, subangular).

### Lithologic and stratigraphic igneous units

#### *Unit III (aphyric to plagioclase[±olivine]-phyric trachybasalt)*

Interval: Sections 330-U1377B-2R-1, 0 cm, to 5R-4, 18 cm

Depth: 9.10–31.98 mbsf

Lithologic units: 1–18

The igneous succession in Hole U1377B consists of only one stratigraphic unit, which is dominantly aphyric with a 3.78 m olivine-plagioclase-phyric and plagioclase-phyric interval in the middle of the recovered section (Fig. F8). As with Hole U1377A, the rocks in Hole U1377B also exhibit flow banding and are therefore also likely to be trachybasalt, even though we have no thin sections or chemical analyses. Postcruise petrographic and analytical studies will allow us to apply more rigorous names to the rock types.

Unit III is made up of 18 lithologic units, the first of which (lithologic Unit 1) is a 10.11 m thick aphyric trachybasalt flow with occasional banding (Fig. F9C), defined by grain size (aphanitic to fine grained) and vesicle abundance (0%–20%), overlying the remainder of the lithologic units comprising a sequence of trachybasalt pillows. Toward the base of lithologic Unit 1 is a 6 cm thick interval of moderately olivine-phyric trachybasalt (interval 330-U1377B-4R-1, 12–18 cm), below which rocks become more veined and finally brecciated. The boundary between lithologic Units 1 and 2 was not recovered.



Lithologic Unit 2 is defined by the appearance of olivine and plagioclase phenocrysts, with the plagioclase sometimes occurring in glomerocrysts with augite. The base of lithologic Unit 2 is defined by a curved glassy margin. Lithologic Units 3, 4, and 5 are thin intervals (0.12, 0.07, and 0.12 m thick, respectively) of plagioclase-phyric trachybasalt, with small amounts of augite phenocrysts and also olivine microphenocrysts. Lithologic Units 3 and 4 are separated by curved glassy margins (Fig. F10). Lithologic Units 4 and 5 have curved lower glassy margins, but contacts with their respective units below were not recovered. Lithologic Unit 6 is 1.18 m thick and composed of vesicular (10%), sparsely plagioclase-phyric trachybasalt. The unit becomes increasingly veined toward its base, and the point where it breaks up into breccia defines the top of lithologic Unit 7, which has the same lithology as the overlying unit. Lithologic Unit 8 is a complicated interval with sparsely plagioclase-phyric trachybasalt clasts in an aphyric matrix that appears to have intruded into the breccia and is glassy in its upper part (Fig. F11). The 1.39 m thick lithologic Unit 9 has a curved glassy base, although its contact with lithologic Unit 10, a breccia composed of aphyric trachybasalt clasts, was not recovered. The boundary between lithologic Units 10 and 11 was also not recovered. Lithologic Units 11, 12, 13, and 14 are composed of aphyric trachybasalt, and all are <1 m thick and separated from each other by curved glassy margins. The lower boundary of lithologic Unit 14 was not recovered. Lithologic Unit 15 is an interval of brecciated aphyric trachybasalt, whereas lithologic Unit 16 is more massive aphyric trachybasalt. Lithologic Unit 17 is 51 cm thick and composed of aphyric trachybasalt with bands of vesicles. Its upper contact consists of a narrow glassy body that appears to protrude into lithologic Unit 16 (Fig. F12). The boundary between lithologic Units 17 and 18 is another curved glassy margin across which the lithology does not change. Drilling ended at 37.0 mbsf, 1.44 m into lithologic Unit 18.

### Interpretation of the igneous succession at Site U1377

The igneous successions cored in Holes U1377A and U1377B are broadly similar in lithology. Both consist largely of aphyric trachybasalt with occasional olivine-rich bands, and Hole U1377B contains intervals with plagioclase-augite glomerocrysts. The presence of flow banding in all of the Hole U1377A succession and in the upper part of Hole U1377B suggests that these parts of the successions formed as massive lava flows or smaller lobate flows. There is no evidence in these flows that allows us to determine whether they

were erupted in a submarine or subaerial environment. The lower part of the succession in Hole U1377B, however, consists of much smaller (7 cm to 2.08 m) individual cooling units with well-preserved curved glassy margins (Fig. F10), suggesting that they are small lobate flows or lava pillows emplaced in a submarine environment. A curious feature of these margins is that, in several instances, glass between adjacent pillows connects with the more massive interior of a pillow below (Figs. F11, F12). It appears that, while in the still molten interior of a pillow, lava broke out as a protrusion that filled the space between overlying pillows. Alternatively, magma may have been injected into a stack of pillows; however, the similarity in appearance between the injected and pillow trachybasalt suggests that both were part of the same eruptive event. The presence of glassy pillow margins that are distinct from the glass in the protrusion (e.g., Fig. F10) shows that the pillows must have had glassy crusts when lava from below protruded into the space between them. In one case, fragments of the pillows themselves are incorporated into the protrusion (Fig. F11). The observation of three examples of magma apparently intruding upward into the spaces between overlying pillows suggests that this was a common phenomenon at Site U1377.

Time constraints limited the shipboard petrographic and geochemical investigation of the lithologic units at Site U1377, so we have to infer the rock composition from visual inspection of the core. However, it seems likely that the magma represented by the rocks recovered at this site was generally alkalic and intermediate in composition. If postexpedition petrographic and analytical studies confirm this, then the rocks recovered at Site U1377 will have the most evolved composition of all the rocks drilled during Expedition 330.

## Alteration petrology

Three stratigraphic units (including six lithologic units) were identified in cores from Hole U1377A, and another three stratigraphic units (comprising 18 lithologic units) were recognized in cores from Hole U1377B (see “[Igneous petrology and volcanology](#)”). The entire section of trachybasaltic rocks at Site U1377 has undergone some degree of alteration by low-temperature water-rock interaction.

The overall alteration of volcanic rocks from Hole U1377A ranges from nearly fresh to highly altered (10%–95%) and from slightly to completely altered for rocks from Hole U1377B (Fig. F13). No evidence of greenish alteration indicative of reducing conditions was observed in either Holes U1377A or

U1377B. Rather, it appears that oxidizing conditions were prevalent. Alteration at Site U1377 resulted in replacement of olivine and volcanic glass in some rocks. Olivine is altered to green and white clay in Hole U1377A but to iddingsite and Fe oxyhydroxides in Hole U1377B (Fig. F14).

### Alteration phases

We distinguished three main groups of alteration minerals in Holes U1377A and U1377B:

1. Carbonates are abundant secondary minerals as infillings in vesicles and veins. X-ray diffraction analyses on veins and vesicles suggest Mg calcite is predominant, with siderite and ankerite also being present (Fig. F15).
2. Clay minerals (mostly white clay) are also abundant secondary phases and were principally identified using optical microscopy.
3. Other secondary phases are pyrite (especially in lithologic Units 4–6 in Hole U1377A; Fig. F16), Mn oxides, and various Fe oxyhydroxides, likely hematite and goethite.

### Overall alteration characteristics of Hole U1377A

The overall alteration of volcanic rocks in Hole U1377A is dominantly slight to moderate but has an overall range from fresh to high (10%–75%), as estimated from core descriptions and thin section observations (Fig. F13). Pervasive alteration imparted a brownish to brownish-gray color to the rocks (Figs. F13, F17). Moderately fresh rock with <20% altered groundmass is present in Sections 330-U1377A-3R-2, 6R-2, and 6R-3.

Olivine is typically completely altered to white clay in the trachybasalt from Hole U1377A (Fig. F14). Augite is not abundant and may have minor amounts of clay along fractures (Sample 330-U1377A-3R-2, 2–4 cm [Thin Section 270]). Vesicles are mostly filled with carbonate and white clay (Fig. F18). Abundant veins are present in these rocks. These veins are mostly filled with Fe oxyhydroxides in the uppermost 16 mbsf and with carbonates, white clay, and minor amounts of Fe oxyhydroxides in the remainder of the core (Fig. F19).

### Overall alteration characteristics of Hole U1377B

The overall degree of alteration of the 18 lithologic units in Hole U1377B is high (>50%). Only a few intervals are slightly to moderately altered (e.g., Section 330-U1377B-4R-2 and interval 4R-3, 21–141 cm), and a few are completely altered (e.g., interval 4R-1, 0–12 cm). Alteration colors are brown to red-

dish brown, with strong evidence of oxidation. Olivine is altered to iddingsite and Fe oxyhydroxides. Plagioclase shows minor alteration to sericite/illite in some rocks but characteristically is fresh.

The overall high amount of alteration generally has completely transformed glass, but moderately fresh glass is present along what appear to be pillow rinds in intervals 330-U1377B-4R-3, 120–135 cm; 4R-4, 1–10 cm; 4R-5, 6–15 cm; and 5R-2, 96–110 cm. These are elongated glassy bands up to 15 cm long and ~1–2 cm wide.

Two dominant types of vein-fill minerals were identified. Carbonates and Fe oxyhydroxides form their own distinct veins, but many are composite, having both minerals present. Composite veins are typically >1 mm thick.

### Vesicle infillings

Vesicles in rocks from Hole U1377A contain mainly carbonates and green and white clay minerals (Fig. F18). Thin section observations indicate a mixture of both in many vesicles, with smectite at the rim and carbonate in the interiors (Fig. F16A, F16B). The carbonate infilling may be zoned (Fig. F20), which may indicate precipitation of carbonate from different fluid compositions or temperatures. In this interval, we also observed pyrite in the groundmass and as coatings in vesicles that were later filled with carbonates (Fig. F20). X-ray diffraction patterns of the infilling of these vesicles identified the carbonates as Mg calcite, ankerite, and siderite (Fig. F15).

Vesicles in the rocks from Hole U1377B are quite similar, with carbonates and clay minerals as the dominant infilling minerals. Fe oxyhydroxide minerals are also present.

### Vein infillings

In the cores from Hole U1377A, a total of 178 veins and vein networks were measured by the structural geologists, yielding an average of 4 veins per meter (see “Structural geology”). Most veins are quite thin and consist of carbonate and clay (Fig. F19). For Hole U1377B, the structural geologists measured 283 veins and vein networks, with an average of 9 veins per meter. The veins contain mainly carbonate interiors and reddish Fe oxyhydroxides (goethite) margins (Figs. F16C, F16D, F19). Many of the veins and fractures have reddish alteration halos. Other veins contain small dark minerals and dendrites, suggesting the presence of Mn oxides.

### Interpretation of alteration

Igneous units throughout Holes U1377A and U1377B are affected by multistage alteration, mainly

dominated by low-temperature fluid-rock interactions. The abundance of smectite and carbonates throughout Site U1377 indicates low temperatures (30°–150°C) typical of the lowest stages of ocean crust alteration (Alt, 1995). Ankerite and siderite were observed in Hole U1377A. These minerals are stable over a wide range of temperatures but can form at relatively low temperatures (<85°C). Nevertheless, they are not very common in the oceanic crust because they are metastable and can be easily dissolved (Laverne, 1993). Additionally, the number of veins filled with Fe oxyhydroxides (e.g., goethite) in Hole U1377B suggests alteration under oxidizing conditions (and probably weathering) or at least alteration in a shallow-water environment.

Combining observations from the two holes at Site U1377, we propose a two-stage alteration process similar to that discussed by Laverne (1993). The first stage would have taken place under reducing conditions, where the hydrothermal fluids penetrated the basalt and precipitated pyrite and siderite and probably Mn oxides. In a second stage under more oxidizing conditions, Fe oxyhydroxides precipitated and red halos formed.

## Structural geology

Structures observed, measured, and described at Site U1377 on Hadar Guyot are geopetals, veins, vein networks, fractures, vesicle bands, and igneous contacts (Fig. F21). The characteristics, orientations, and distribution of these structures at Site U1377 are described below.

In Hole U1377A, veins ( $N = 135$ ; 208 individual features), vein networks ( $N = 43$ ; 358 individual veinlets), and vesicle bands ( $N = 38$ ) are the dominant structural features (Fig. F21A). These features are also dominant in Hole U1377B, where 224 veins (306 individual features), 59 vein networks (432 individual features), and 38 vesicle bands were recorded (Fig. F21B).

Veins are abundant in the recovered basement from both Holes U1377A and U1377B (Fig. F22). The highest vein density (34 veins per meter) in Hole U1377A was observed at 15.1–16.6 mbsf (lithologic Unit 1), whereas most of the recovered intervals have 5–25 veins per meter. In Hole U1377B, the maximum vein density is 26 veins per meter at 20–21 mbsf (lithologic Unit 2), whereas other recovered intervals typically have 10–24 veins per meter. Average vein widths in Holes U1377A and U1377B are 0.6 and 1.1 mm, and the maximum vein widths in these holes are 9 and 12 mm, respectively. Thus, Site U1377 has a similar average vein width to Sites U1372, U1373, and U1374 but smaller average width

compared to Site U1376. The vein density at Site U1377 is intermediate between Site U1376 (which has a very high vein density) and the other Louisville sites (which have generally lower vein densities), indicating only intermediate amounts of fluid flow in this part of Hadar Guyot compared to the other sites. The veins are moderately to steeply dipping in both Holes U1377A and U1377B (Fig. F23A, F23D).

Fractures are sparse at Site U1377, with only five observed in Hole U1377A and none observed in Hole U1377B (Fig. F21). In Hole U1377A they occur in the aphyric rocks of lithologic Unit 3, with three oriented features having moderately steep dips of 50°–60° (Fig. F23B).

In Hole U1377B a single horizontal geopetal structure is present at 0.8 mbsf (Fig. F24), providing evidence that this part of Hadar Guyot has not been tilted since deposition of the geopetal infilling material.

The lower part of Hole U1377B has several glassy chilled margins that are interpreted as the quenched rims of pillow lavas (see “[Igneous petrology and volcanology](#)”). These chilled margins have moderate to steep dips that range from 45° to 90° (Fig. F23E). Subparallel to these chilled margins are zones of vesicle banding (Fig. F10), which also yield moderate to steep dips (Fig. F23F).

Two zones of glass in Hole U1377B do not simply represent quenching on pillow rims. In interval 330-U1377B-5R-2A, 96–114 cm (Fig. F12), moderately dipping vesicle bands on the top right of the image are truncated by glassy material. This glass progressively grades into more crystalline material toward the base of this interval, with vesicle banding parallel to the edges of the glass. This crosscutting relationship indicates that molten material from below was intruded into the rock above. In interval 330-U1377B-4R-5A, 1–34 cm, angular fragments of trachybasalt are surrounded by glassy material (Fig. F11). Both of these examples indicate forceful injection of magma after the surrounding material cooled. Although these particular lithologic units have not yet been analyzed chemically, this behavior may be a result of the more evolved—and therefore more viscous—magma (of trachybasalt composition) found elsewhere at Site U1377 (see “[Geochemistry](#)”).

Vesicle bands in Hole U1377A are typically steeply dipping or subhorizontal (Fig. F23C). The vesicle bands in Hole U1377A are visually similar to those recorded in Hole U1377B, with the exception that no glassy chilled margins were found. The vesicle bands in Hole U1377A were potentially formed in the same manner as those in Hole U1377B (as pil-

lows), but chilled margins were not recovered because of the low recovery in Hole U1377A.

## Summary

Structural features at Site U1377 are dominated by veins, with as many as 34 and 26 veins per meter recorded in Holes U1377A and U1377B, respectively. The average vein widths in Holes U1377A and U1377B are 0.6 and 1.1 mm, respectively, and the maximum vein widths are 9 and 12 mm. Site U1377 therefore has similar vein widths as Sites U1372, U1373, and U1374 (but with somewhat higher vein density than these sites) and fewer and smaller veins than Site U1376. The veins have moderate to steep dips in both Holes U1377A and U1377B. A single horizontal geopetal structure at 0.8 mbsf in Hole U1377A provides evidence that this part of Hadar Guyot has not been tilted since deposition of the geopetal infilling material. In Hole U1377B glassy chilled contacts and vesicle bands have moderate to steep dips. Glass also occurs in Hole U1377B along the edge of a small intrusion as well as in the matrix of a breccia, indicating the forceful local injection and rapid cooling of new magma of trachybasalt composition into already solidified rocks.

## Geochemistry

### Igneous rocks

Concentrations of major elements and several trace elements (Table T7) were measured for one Site U1377 sample by inductively coupled plasma-atomic emission spectroscopy (see “Geochemistry” in the “Methods” chapter [Expedition 330 Scientists, 2012a], for information on analytical procedures, instrumentation, and data quality). This sample (330-U1377A-3R-2 [Piece 1, 2–4 cm]) is from a moderately olivine-phyric lava flow of stratigraphic Unit III.

The total for the major element oxides is 98.68 wt%. As with other Expedition 330 analyses, we normalized the raw major element values to a 100 wt% total. The normalized values are presented below the raw data in Table T7 and are used in figures in the “Site U1376” chapter (Expedition 330 Scientists, 2012c) and in the discussion below.

Weight loss on ignition (LOI) is 3.0 wt%, indicating a relatively high level of alteration, consistent with petrographic observations (see “Alteration petrology” and “Igneous petrology and volcanology”). The LOI measurement was made after the chemical analysis, contrary to the procedure explained in “Geochemistry” in the “Methods” chapter (Expedition 330 Scientists, 2012a). This was a time-saving measure that allowed us to include the sample in the fi-

nal batch of powders analyzed during the expedition.

Silica concentration is 55.00 wt%, the highest encountered at any of the Expedition 330 sites. In a total alkalis ( $\text{Na}_2\text{O} + \text{K}_2\text{O}$ ) vs.  $\text{SiO}_2$  diagram, data for the sample fall in the field of basaltic trachyandesite, very close to the line dividing alkalic and tholeiitic compositions (see Fig. F38 in the “Site U1376” chapter [Expedition 330 Scientists, 2012c]). However, neither the alteration-resistant elements nor the mineralogy of the rock (see “Igneous petrology and volcanology”) provides any evidence of tholeiitic affinities, and it is likely that alteration has modified the sample’s  $\text{K}_2\text{O}$  and possibly  $\text{Na}_2\text{O}$  concentration. Concentrations of incompatible elements much less susceptible (Zr and  $\text{TiO}_2$ ) or generally less susceptible (Sr,  $\text{P}_2\text{O}_5$ , and Ba) to alteration than  $\text{K}_2\text{O}$  are near the high end of values measured for other Expedition 330 samples (e.g., Fig. F40A–F40C in the “Site U1376” chapter [Expedition 330 Scientists, 2012c]). This characteristic suggests that the rock represents highly differentiated alkalic to transitional magma that evolved from a more mafic composition rather like those samples cored at other Expedition 330 sites. Yttrium concentration is relatively low (see Fig. F40D in the “Site U1376” chapter [Expedition 330 Scientists, 2012c]).

Major element characteristics are also consistent with highly differentiated magma. In addition to high  $\text{SiO}_2$ , the sample has the highest  $\text{Al}_2\text{O}_3$  (18.65 wt%), the lowest  $\text{Fe}_2\text{O}_3^{\text{T}}$  (7.01 wt%; the superscript indicates total iron as  $\text{Fe}_2\text{O}_3$ ), and the second-lowest MgO (3.00 wt%), CaO (6.18 wt%), and CaO/ $\text{Al}_2\text{O}_3$  (0.33) values of the Expedition 330 samples (see Fig. F39 in the “Site U1376” chapter [Expedition 330 Scientists, 2012c]). However, several other features are inconsistent with an origin by simple differentiation of a basaltic parent magma. In particular, concentrations of the compatible trace elements Ni (421 ppm), Cr (686 ppm), and Co (122 ppm) are exceptionally high. Such high values are unusual even in basalts, and during Expedition 330 broadly similar concentrations were found only in the highly olivine-phyric high-MgO basalts of Site U1376 (see Table T9 in the “Site U1376” chapter [Expedition 330 Scientists, 2012c]). Mg number ( $\text{Mg\#} = 100 \times \text{Mg}^{2+}/[\text{Mg}^{2+} + \text{Fe}^{2+}]$ , assuming  $\text{Fe}_2\text{O}_3/\text{FeO} = 0.15$ ) also is comparatively high (49.9) for a rock with 55 wt%  $\text{SiO}_2$ , as are V (281 ppm) and Sc (29 ppm) concentrations.

The combined results suggest a relatively complicated petrogenesis, perhaps involving contamination of ascending evolved magma with a small amount of olivine-rich material from ultramafic wall rock or a crystal mush zone. If so, the uncontami-

nated magma would have been even more siliceous than the resulting contaminated mixture. Detailed studies on shore will be required for a fuller understanding of this unusual rock.

### Carbon, organic carbon, nitrogen, and carbonate

No samples from Site U1377 were analyzed for carbonate, total carbon, total organic carbon, or total nitrogen content.

## Physical properties

Characterization of physical properties was conducted on cores recovered from Holes U1377A and U1377B at Hadar Guyot. The whole-round core sections (10 from Hole U1377A and 15 from Hole U1377B, not including sections from ghost Core 330-U1377B-3G) were run through the Whole-Round Multisensor Logger (WRMSL) for measurements of gamma ray attenuation (GRA) bulk density and magnetic susceptibility. Whole-round core sections longer than 50 cm (21 of 25 total sections) were also run through the Natural Gamma Radiation Logger (NGRL). The archive-half split-core sections were run through the Section Half Multisensor Logger (SHMSL) for measurement of laser height, color reflectance, and point magnetic susceptibility. Moisture and density measurements were performed on six discrete samples from Hole U1377A only. Compressional wave (*P*-wave) velocity was measured in three orthogonal directions on 13 discrete oriented rock cubes, including seven samples selected from Hole U1377B. These samples were also used for paleomagnetic measurements of alternating-field demagnetization (see “[Paleomagnetism](#)”). Because of equipment failure, no measurements of thermal conductivity were made at this site (see “[Physical properties](#)” in the “Methods” chapter [Expedition 330 Scientists, 2012a]). No physical property measurements were made on ghost Core 330-U1377B-3G (see “[Operations](#)”).

### Whole-Round Multisensor Logger measurements

Throughout the lithified sediments and igneous rocks of Holes U1377A and U1377B the core is fractured and broken, as is typical of hard rock coring. These discontinuities in the recovered core led to spurious values in the data collected with the WRMSL and SHMSL, so we applied a data filtering and processing algorithm to remove the affected data (see “[Physical properties](#)” in the “Methods” chapter [Expedition 330 Scientists, 2012a]). In this

report we show only the filtered data; for raw data we refer the reader to the visual core descriptions (see “[Core descriptions](#)”) and the Laboratory Information Management System (LIMS) database ([iodp.tamu.edu/tasapps/](http://iodp.tamu.edu/tasapps/)).

### Magnetic susceptibility

Whole-round magnetic susceptibility measurements for the two holes from Site U1377 are shown in Figure F25. Magnetic susceptibility is sensitive to the mineralogical composition of the rock. Hole U1377A magnetic susceptibility averages  $8.42 \times 10^{-3}$  SI, and Hole U1377B averages  $3.75 \times 10^{-3}$  SI. Although magnetic susceptibility is highly variable throughout both holes, three intervals of markedly higher values exceeding  $2.50 \times 10^{-2}$  SI were observed: 25–27 mbsf and 35–36.5 mbsf for Hole U1377A and 12–12.5 mbsf for Hole U1377B. All of these intervals are associated with aphyric trachybasalts (see “[Igneous petrology and volcanology](#)”). No distinct patterns in other types of physical property data were observed at these specific depths.

### Gamma ray attenuation bulk density

The results of GRA-derived bulk density for the two holes are shown in Figure F25. A correction factor of 1.138 was applied to account for the average diameter of the hard rock cores (58 mm) being less than the full 66 mm diameter of the core liner (see “[Physical properties](#)” in the “Methods” chapter [Expedition 330 Scientists, 2012a]). Values of  $<1.00$  g/cm<sup>3</sup> were attributed to empty portions of core liner and removed. The average GRA-derived bulk densities of Holes U1377A and U1377B are 2.24 g/cm<sup>3</sup> and 2.33 g/cm<sup>3</sup>, respectively.

For Hole U1377A, average GRA-derived bulk density increases from 1.90 g/cm<sup>3</sup> at 15.3–16.7 mbsf to 2.41 g/cm<sup>3</sup> at 43.9–47.2 mbsf, near the bottom of the hole. Two high values averaging 2.60 g/cm<sup>3</sup> found at ~6.2 mbsf are likely associated with a piece of limestone with ferromanganese encrustation on its top recovered in Section 330-U1377A-2R-1.

The GRA-derived bulk density profile for Hole U1377B is characterized by relatively low values near the top, representing foraminiferal ooze, and an interval from 19.5 to 21.3 mbsf with an average value of 2.72 g/cm<sup>3</sup>, an increase over the background average of 2.40 g/cm<sup>3</sup> for igneous sections recovered deeper than 9 mbsf. This group of high density measurements corresponds with the olivine-plagioclase-phyric trachybasalt of lithologic Unit 2. The overall density of igneous units is lower than that observed at earlier Expedition 330 sites, possibly reflecting the

increased silica content of these magmas (see “[Geochemistry](#)”).

### Natural Gamma Radiation Logger

Natural gamma radiation (NGR) measurements reflect the amount of uranium, thorium, and potassium present in the rock. Results from the NGRL are shown in Figure [F25](#). Low NGR was measured in the foraminiferal ooze of Hole U1377B, as would be expected for calcareous sand. However, NGR for igneous rocks from both Holes U1377A and U1377B is quite high relative to previous Expedition 330 sites, with averages of 20.00 counts per second (cps) and 22.58 cps, respectively. For Hole U1377A, NGR ranges from 7.36 to 42.17 cps, with the highest values appearing at 45 mbsf, corresponding with the olivine-phyric trachybasalt of lithologic Units 4–6 (see “[Igneous petrology and volcanology](#)”). The igneous rocks of Hole U1377B exhibit a similar NGR range of 3.90–45.52 cps. High NGR (>30 cps) was measured at ~18.5 mbsf, 21.4–24.3 mbsf, and 28.0–28.7 mbsf. These large values may reflect increased alteration compared to other sites or could be related to a more evolved magma composition (see “[Geochemistry](#)”).

### Section Half Multisensor Logger measurements

#### Color reflectance spectrometry

Color reflectance spectrometry results showing values of  $L^*$ , which corresponds to lightness, and  $a^*$  and  $b^*$ , which correspond to redness versus greenness and yellowness versus blueness, respectively, are summarized in Figure [F26](#). The uppermost data points for  $L^*$  in Hole U1377A (6.12–6.19 mbsf) exhibit considerable variability over this narrow interval, with some values of >70. These high values correspond to the small piece of limestone encrusted with ferromanganese oxides recovered in Section 330-U1377A-2R-1. In the igneous basement of Hole U1377A the majority of  $L^*$  values fall between 25 and 50, with a slight increase downhole.  $L^*$  values from Hole U1377B have a similar pattern, with high values around 75 at the top, corresponding to an interval of light-colored foraminiferal ooze, and most of the remaining values in the igneous basement falling between 25 and 50, with no significant downhole trend.

Values of  $a^*$  for Hole U1377A indicate a tendency toward a red spectrum above ~17 mbsf but are generally neutral in the rest of the hole. Color reflectance values for  $b^*$  are also quite neutral for Hole U1377A, except for the interval from 15 to 17 mbsf, which shows a moderately yellow spectrum. Values of both

$a^*$  and  $b^*$  are consistently positive for Hole U1377B, indicating a strongly red and yellow color reflectance spectrum. This strong redness and yellowness is likely related to intense alteration by oxidation apparent along cracks and veins and throughout much of the rock recovered from this hole (see “[Alteration petrology](#)”).

#### Point magnetic susceptibility

Point magnetic susceptibility results are shown in Figure [F25](#), along with whole-round magnetic susceptibility data. The pattern of peaks and troughs is consistent between the two data sets; however, point magnetic susceptibility has a consistently lower average than whole-round magnetic susceptibility. Hole U1377A has an average point magnetic susceptibility of  $5.76 \times 10^{-3}$  SI, and Hole U1377B has an average of  $2.31 \times 10^{-3}$  SI.

#### Moisture and density

Results of bulk density, dry density, grain density, void ratio, water content, and porosity measurements on discrete samples from Hole U1377A are listed in Table [T8](#). Moisture and density measurements on discrete samples were not performed for Hole U1377B because time constraints at the end of the expedition did not allow for the ~50 h measurement procedure. Bulk density in Hole U1377A ranges from 2.19 to 2.53 g/cm<sup>3</sup>, with an average of 2.43 g/cm<sup>3</sup>. Porosity ranges from 16.7% to 33.2%, with an average of 23.5%. Figure [F25](#) shows the variation of bulk density with depth based on both discrete samples (Hole U1377A only) and GRA-derived bulk density and further illustrates the strong correlation between the two. Figure [F25](#) shows the variation of porosity with depth for Hole U1377A. Density and porosity are strongly correlated, suggesting that changes in porosity, rather than in composition, are the primary cause of the variations in density.

#### Compressional wave (*P*-wave) velocity

Compressional wave (*P*-wave) velocity was measured on discrete samples in three orthogonal directions: along the  $x$ -axis normal to the split-core surface, along the  $y$ -axis parallel to the split-core surface, and along the  $z$ -axis downcore. *P*-wave velocity measurements were performed for Hole U1377A on the same discrete samples used for moisture and density testing. For Hole U1377B, discrete oriented rock cubes were selected in collaboration with the paleomagnetism laboratory group, with *P*-wave testing to be performed following alternating-field demagnetization. Downhole variations in *P*-wave velocity for Holes U1377A and U1377B are shown in Figure [F25](#) and

Table T8. Measured values for Hole U1377A range from 3.22 to 4.39 km/s (average = 3.87 km/s), and those for Hole U1377B range from 3.21 to 4.71 km/s (average = 4.06 km/s). *P*-wave velocities are generally consistent throughout both holes. The values are typically lower than those observed in lavas at previous sites, possibly reflecting the more evolved composition of these magmas or increased alteration (see “[Geochemistry](#)”).

## Paleomagnetism

Holes U1377A and U1377B had only shallow penetration and, particularly for Hole U1377A, poor core recovery. Nonetheless, samples from both holes appear to have moderate to steep positive inclinations, indicating Southern Hemisphere reversed polarity. Shipboard sampling at these holes was limited because of the short time remaining for shipboard analysis by the end of the expedition.

### Archive-half core remanent magnetization data

The remanent magnetization of the archive halves of Cores 330-U1377A-3R through 6R and 330-U1377B-2R, 4R, and 5R was measured at 2 cm intervals using the cryogenic magnetometer. All data acquired within 4.5 cm of either piece end were filtered out prior to further processing, and thus only pieces longer than 9 cm were considered. No core pieces in the sedimentary units were suitable for measurement, and no measurements were made for ghost Core 330-U1377B-3G.

The natural remanent magnetization (NRM) intensity at Site U1377 is lower than at previous guyots sampled during Expedition 330. The average NRM intensity is <1 A/m (Fig. F27B). These low NRM values may be related to the high degree of alteration (see “[Alteration petrology](#)”).

Best-fit principal component directions were calculated from alternating-field (AF) demagnetization data for each 2 cm interval of the archive halves using an automated routine that maximizes the percentage of remanence incorporated and minimizes the scatter about the best-fit direction and the deviation of this vector from the origin (see “[Paleomagnetism](#)” in the “[Methods](#)” chapter [Expedition 330 Scientists, 2012a]). Based on the distribution of misfit values, only directions with misfit values below 2.42 for Hole U1377A and 1.89 for Hole U1377B were considered; these represent the most reliable 40% of the total number of 2 cm interval principal component directions for each hole. These misfit values are lower than those used for Sites U1372,

U1373, and U1374, where the misfit cutoff value was set at ~3.4. The resulting inclinations, intensities, and stability of remanent magnetization, as represented by the median destructive field (MDF'), are shown in Figure F27. Although Site U1377 is dominated by positive inclinations, indicative of Southern Hemisphere reversed polarity (Fig. F27D), the shallow penetration and low recovery limit recognition of any inclination trends with depth or lithology.

### Discrete sample remanent magnetization data

The remanent magnetization of 17 discrete basalt samples (10 from Hole U1377A and 7 from Hole U1377B) was measured with the spinner magnetometer. NRM intensities range more widely in Hole U1377B ( $1.35 \times 10^{-2}$  to 3.99 A/m) than in Hole U1377A (0.13 to 1.86 A/m) (Fig. F28; Table T9). Königsberger ratio ( $Q_n$ ) values for Hole U1377A samples are typically >1, but those for Hole U1377B display a broader range, with a minimum of 0.18 and a maximum of 8.90.

Ten discrete samples from Hole U1377A were demagnetized, six by AF demagnetization and four by thermal demagnetization (Table T9; Fig. F29). Only AF demagnetization was attempted for discrete samples from Hole U1377B because of the limited time. Unfortunately, all seven discrete samples from Hole U1377B were remagnetized by a malfunction of the demagnetizer DTech 2000, and no characteristic remanent magnetization directions were obtained. The demagnetization results from basalt samples reveal relatively simple behavior and are generally, though not always (see below), consistent with the moderate to steep positive inclinations observed in the archive-half data. Although only limited thermal demagnetization data are available, results from thermal and AF demagnetization apparently recover the same magnetization component (Fig. F29B, F29C). The coercivity of the discrete samples from Site U1377 is generally lower than for previous sites (Fig. F29).

### Anisotropy of magnetic susceptibility

The anisotropy of magnetic susceptibility was determined for all discrete samples (Table T10). The average degree of anisotropy ( $P'$ ) is 1.01, and shape factors ( $T$ ) range from -0.49 to 0.72 (where  $T = -1$  if prolate and  $T = 1$  if oblate; Jelinek, 1981).

## Discussion

Inclinations at Site U1377 are uniformly positive (reversed polarity; Fig. F30; Table T11) but are more

variable than those observed at some other sites (e.g., U1374 and U1376). This variability suggests that the pillows/lava lobes reflect accumulation over some significant amount of time. Discrete sample inclinations in some cases do not agree well with archive-half results (e.g., Cores 330-U1377A-4R and 5R). This discrepancy will be the subject of shore-based studies. Any inferences about the paleolatitude of Site U1377 should be undertaken with care, given the limited penetration and core recovery.

## Microbiology

The goals of microbiology sampling at Site U1377 were to collect samples for shore-based cell counts, molecular biological analyses, and  $\delta^{34}\text{S}$  and  $\delta^{13}\text{C}$  stable isotope analyses; to inoculate media for cultivation of seafloor microbes; and to set up stable isotope addition bioassays whereby the rate of incorporation of compounds labeled with  $^{14}\text{C}$ ,  $^{15}\text{N}$ , and  $^{34}\text{S}$  can be measured. Such bioassays will allow calculation of metabolic rates of seafloor microbes at Hadar Guyot. Two whole-round samples (8–11 cm long) were collected for microbiological analysis: a moderately olivine-phyric trachybasalt from 46.84 mbsf in Hole U1377A and an aphyric trachybasalt from 18.1 mbsf in Hole U1377B (Fig. F31). Both samples were preserved for shore-based DNA analysis, cell counting, and  $\delta^{34}\text{S}$  and  $\delta^{13}\text{C}$  analyses. Sample 330-U1377B-4R-1, 0–8 cm, was used to inoculate 18 culturing experiments with nine different types of cultivation media (Table T12). Both samples were used to set up stable isotope addition bioassays to determine rates of carbon, nitrogen, and sulfur utilization by subsurface microbes at Hadar Guyot (Table T13). A sample of drill fluid was collected for analysis of the microbial community for comparison with microbial communities in the subsurface rocks collected and for detection of possible contamination.

### Culturing experiments

Sample 330-U1377B-4R-1, 0–8 cm, was used to inoculate 18 culturing experiments with nine different types of cultivation media targeting autotrophic sulfur oxidizers, heterotrophic sulfur oxidizers, autotrophic iron oxidizers, autotrophic iron reducers, heterotrophic iron reducers, and nonspecific heterotrophs (Table T12; for details on media recipes, see Table T14 in the “Methods” chapter [Expedition 330 Scientists, 2012a]). Visual observation of turbidity to assess growth was not carried out because the experiments were inoculated shortly before the end of the cruise and there was not enough time for detectable growth

to occur. All experiments will be analyzed during shore-based research.

### Stable isotope addition bioassays

Both samples collected were used to initiate stable isotope addition bioassays to study rates of carbon, nitrogen, and sulfur cycling by subsurface microbes at Hadar Guyot (Table T13). Enhanced extraction (see “Microbiology” in the “Methods” chapter [Expedition 330 Scientists, 2012a]) was carried out on both samples.

For both samples, 2.71 mM  $^{13}\text{C}$  bicarbonate, 300  $\mu\text{M}$   $^{34}\text{S}$  elemental sulfur, and 0.5  $\mu\text{M}$   $^{15}\text{N}$  ammonia were added to the bioassays (Table T13). Both bioassays included “killed” control vials. These vials were treated in the same way as the other experimental vials, with the exception that after the rock chips were added the vials were combusted at  $>400^\circ\text{C}$  for 3 h to kill all microbes. After the vials were cooled to room temperature, basic seawater media (see “Microbiology” in the “Methods” chapter [Expedition 330 Scientists, 2012a]) and stable isotopes were added to the vials, and from that point on the killed vials were treated like the other (“live”) vials. This kill treatment acts as a negative control and provides a baseline stable isotope reading for the rocks in the experiment. One vial will be terminated at  $t_2$  (2 months; Sample 330-U1377A-6R-3, 56–66 cm, only) and one will be terminated at  $t_3$  (6 months; both samples).

As with the stable isotope addition bioassays performed at other sites, stable isotopes and rock chips were added to 125 mL serum vials, followed by 100 mL of basic seawater media. The vials were then placed in a  $4^\circ\text{C}$  incubator in the dark. At time points of 2 weeks ( $t_1$ ), 2 months ( $t_2$ ), and 6 months ( $t_3$ ), the incubation in one or more vials (depending on number of vials per condition) will be terminated, and the rocks will be collected to measure incorporation of labeled carbon, nitrogen, and sulfur.

### Contamination testing

Drill fluid was collected from a tap located on the drill rig floor, and 2 L of the fluid was filtered onto a 0.2  $\mu\text{m}$  polycarbonate filter. The filter will be analyzed for microbial community composition during shore-based research. Drill fluid is composed primarily of surface seawater that is circulated down through the borehole, and it is unlikely that microbes resident in surface seawater would also be present in the deep subsurface of a seamount. If microbes detected in the drill fluid are also detected in one or more samples, we will know that these samples were most likely contaminated. The Site U1377



drill fluid sample will complement the drill fluid sample collected at Site U1374 (see the “[Site U1374](#)” chapter [Expedition 330 Scientists, 2012b]) for the same type of analysis.

## References

- Alt, J.C., 1995. Subseafloor processes in mid-ocean ridge hydrothermal systems. In Humphris, S.E., Zierenberg, R., Mullineaux, L., and Thomson, R. (Eds.), *Seafloor Hydrothermal Systems: Physical, Chemical, Biological and Geological Interactions within Hydrothermal Systems*. Geophys. Monogr., 91:85–114.
- Arason, P., and Levi, S., 2010. Maximum likelihood solution for inclination-only data in paleomagnetism. *Geophys. J. Int.*, 182(2):753–771. doi:10.1111/j.1365-246X.2010.04671.x
- Beier, C., Vanderkluyzen, L., Regelous, M., Mahoney, J.J., and Garbe-Schönberg, D., 2011. Lithospheric control on geochemical composition along the Louisville Seamount Chain. *Geochem., Geophys., Geosyst.*, 12:Q0AM01. doi:10.1029/2011GC003690
- Cheng, Q., Park, K.-H., Macdougall, J.D., Zindler, A., Lugmair, G.W., Hawkins, J., Lonsdale, P., and Staudigel, H., 1987. Isotopic evidence for a hot spot origin of the Louisville Seamount Chain. In Keating, B.H., Fryer, P., Batiza, R., and Boehlert, G. (Eds.), *Seamounts, Islands and Atolls*. Geophys. Monogr., 43:283–296.
- Courtillot, V., Davaille, A., Besse, J., and Stock, J., 2003. Three distinct types of hotspots in Earth’s mantle. *Earth Planet. Sci. Lett.*, 205(3–4):295–308. doi:10.1016/S0012-821X(02)01048-8
- Duncan, R.A., Tarduno, J.A., and Scholl, D.W., 2006. Leg 197 synthesis: southward motion and geochemical variability of the Hawaiian hotspot. In Duncan, R.A., Tarduno, J.A., Davies, T.A., and Scholl, D.W. (Eds.), *Proc. ODP, Sci. Results*, 197: College Station, TX (Ocean Drilling Program), 1–39. doi:10.2973/odp.proc.sr.197.001.2006
- Expedition 330 Scientists, 2012a. Methods. In Koppers, A.A.P., Yamazaki, T., Geldmacher, J., and the Expedition 330 Scientists, *Proc. IODP*, 330: Tokyo (Integrated Ocean Drilling Program Management International, Inc.). doi:10.2204/iodp.proc.330.102.2012
- Expedition 330 Scientists, 2012b. Site U1374. In Koppers, A.A.P., Yamazaki, T., Geldmacher, J., and the Expedition 330 Scientists, *Proc. IODP*, 330: Tokyo (Integrated Ocean Drilling Program Management International, Inc.). doi:10.2204/iodp.proc.330.105.2012
- Expedition 330 Scientists, 2012c. Site U1376. In Koppers, A.A.P., Yamazaki, T., Geldmacher, J., and the Expedition 330 Scientists, *Proc. IODP*, 330: Tokyo (Integrated Ocean Drilling Program Management International, Inc.). doi:10.2204/iodp.proc.330.107.2012
- Hawkins, J.W., Lonsdale, P., and Batiza, R., 1987. Petrologic evolution of the Louisville Seamount Chain. In Keating, B.H., Fryer, P., Batiza, R., and Boehlert, G.W. (Eds.), *Seamounts, Islands, and Atolls*. Geophys. Monogr., 43:235–254.
- Jelinek, V., 1981. Characterization of the magnetic fabric of rocks. *Tectonophysics*, 79(3–4):T63–T67. doi:10.1016/0040-1951(81)90110-4
- Koppers, A.A.P., Duncan, R.A., and Steinberger, B., 2004. Implications of a nonlinear  $^{40}\text{Ar}/^{39}\text{Ar}$  age progression along the Louisville Seamount Trail for models of fixed and moving hot spots. *Geochem., Geophys., Geosyst.*, 5(6):Q06L02–Q06L23. doi:10.1029/2003GC000671
- Koppers, A.A.P., Gowen, M.D., Colwell, L.E., Gee, J.S., Lonsdale, P.F., Mahoney, J.J., and Duncan, R.A., 2011. New  $^{40}\text{Ar}/^{39}\text{Ar}$  age progression for the Louisville hotspot trail and implications for inter-hotspot motion. *Geochem., Geophys., Geosyst.*, 12:Q0AM02. doi:10.1029/2011GC003804
- Koppers, A.A.P., Yamazaki, T., and Geldmacher, J., 2010. Louisville Seamount Trail: implications for geodynamic mantle flow models and the geochemical evolution of primary hotspots. *IODP Sci. Prosp.*, 330. doi:10.2204/iodp.sp.330.2010
- Laverne, C., 1993. Occurrence of siderite and ankerite in young basalts from the Galápagos spreading center (DSDP Holes 506G and 507B). *Chem. Geol.*, 106(1–2):27–46. doi:10.1016/0009-2541(93)90164-E
- Pearson, P.N., Olsson, R.K., Huber, B.T., Hemleben, C., and Berggren, W.A. (Eds.), 2006. *Atlas of Eocene Planktonic Foraminifera*. Spec. Publ.—Cushman Found. Foraminiferal Res., 41.
- Smith, W.H.F., and Sandwell, D.T., 1997. Global sea floor topography from satellite altimetry and ship depth soundings. *Science*, 277(5334):1956–1962. doi:10.1126/science.277.5334.1956
- Steinberger, B., 2002. Motion of the Easter hot spot relative to Hawaii and Louisville hot spots. *Geochem., Geophys., Geosyst.*, 3(11):8503–8529. doi:10.1029/2002GC000334
- Steinberger, B., and Antretter, M., 2006. Conduit diameter and buoyant rising speed of mantle plumes: implications for the motion of hot spots and shape of plume conduits. *Geochem., Geophys., Geosyst.*, 7(11):Q11018–Q11042. doi:10.1029/2006GC001409
- Steinberger, B., and Calderwood, A., 2006. Models of large-scale viscous flow in the Earth’s mantle with constraints from mineral physics and surface observations. *Geophys. J. Int.*, 167(3):1461–1481. doi:10.1111/j.1365-246X.2006.03131.x
- Steinberger, B., Sutherland, R., and O’Connell, R.J., 2004. Prediction of Emperor–Hawaii Seamount locations from a revised model of global plate motion and mantle flow. *Nature (London, U. K.)*, 430(6996):167–173. doi:10.1038/nature02660
- Tarduno, J.A., Duncan, R.A., Scholl, D.W., Cottrell, R.D., Steinberger, B., Thordarson, T., Kerr, B.C., Neal, C.R., Frey, F.A., Torii, M., and Carvallo, C., 2003. The Emperor Seamounts: southward motion of the Hawai-

ian hotspot plume in Earth's mantle. *Science*, 301(5636):1064–1069. doi:10.1126/science.1086442

Vanderkluisen, L., Mahoney, J.J., Koppers, A.A., and Lonsdale, P.F., 2007. Geochemical evolution of the Louisville Seamount Chain. *Eos, Trans. Am. Geophys. Union*, 88(52)(Suppl.):V42B-06. <http://www.agu.org/meetings/fm07/waisfm07.html>

Wessel, P., and Kroenke, L.W., 1997. A geometric technique for relocating hotspots and refining absolute plate motions. *Nature (London, U. K.)*, 387(6631):365–369. doi:10.1038/387365a0

**Publication:** 11 February 2012  
**MS 330-108**

**Figure F1.** Bathymetric map of the Louisville Seamount Trail in the southwest Pacific, showing the location of Site U1377 on Hadar Guyot close to the Wishbone Scarp (dashed lines). GMT-generated bathymetric map is based on a combination of SIMRAD EM120 multibeam data collected during the AMAT02RR site survey expedition aboard the R/V *Roger Revelle* and global predicted bathymetry (v8.2) from Smith and Sandwell (1997). The current motion of the Pacific plate is indicated with the black arrow. The map uses a linear projection (i.e., vertical and horizontal scales differ) based on WGS-84.

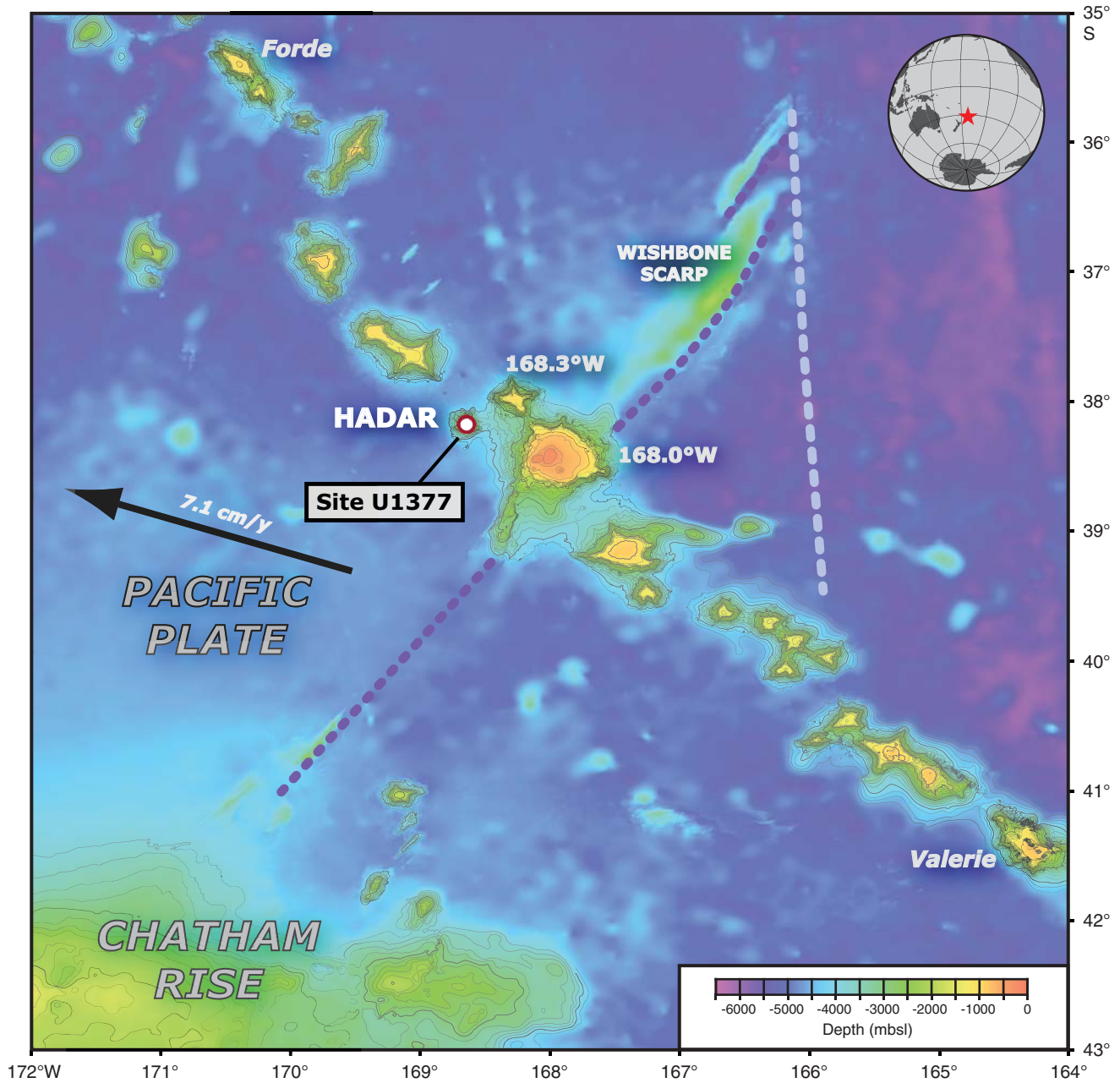


**Figure F2.** Detailed bathymetric map of Site U1377 on Hadar Guyot. GMT-generated bathymetric map is based on SIMRAD EM120 multibeam data collected during the AMAT02RR site survey expedition aboard the R/V *Roger Revelle* and is merged with global predicted bathymetry (v8.2) from Smith and Sandwell (1997). A single dredge location from a previous site survey cruise is indicated by an open square. Crossing multichannel seismic reflection lines collected during the AMAT02RR site survey are shown in blue (for details, see Koppers et al., 2010). Map uses a linear projection (i.e., vertical and horizontal scales differ) based on WGS-84.

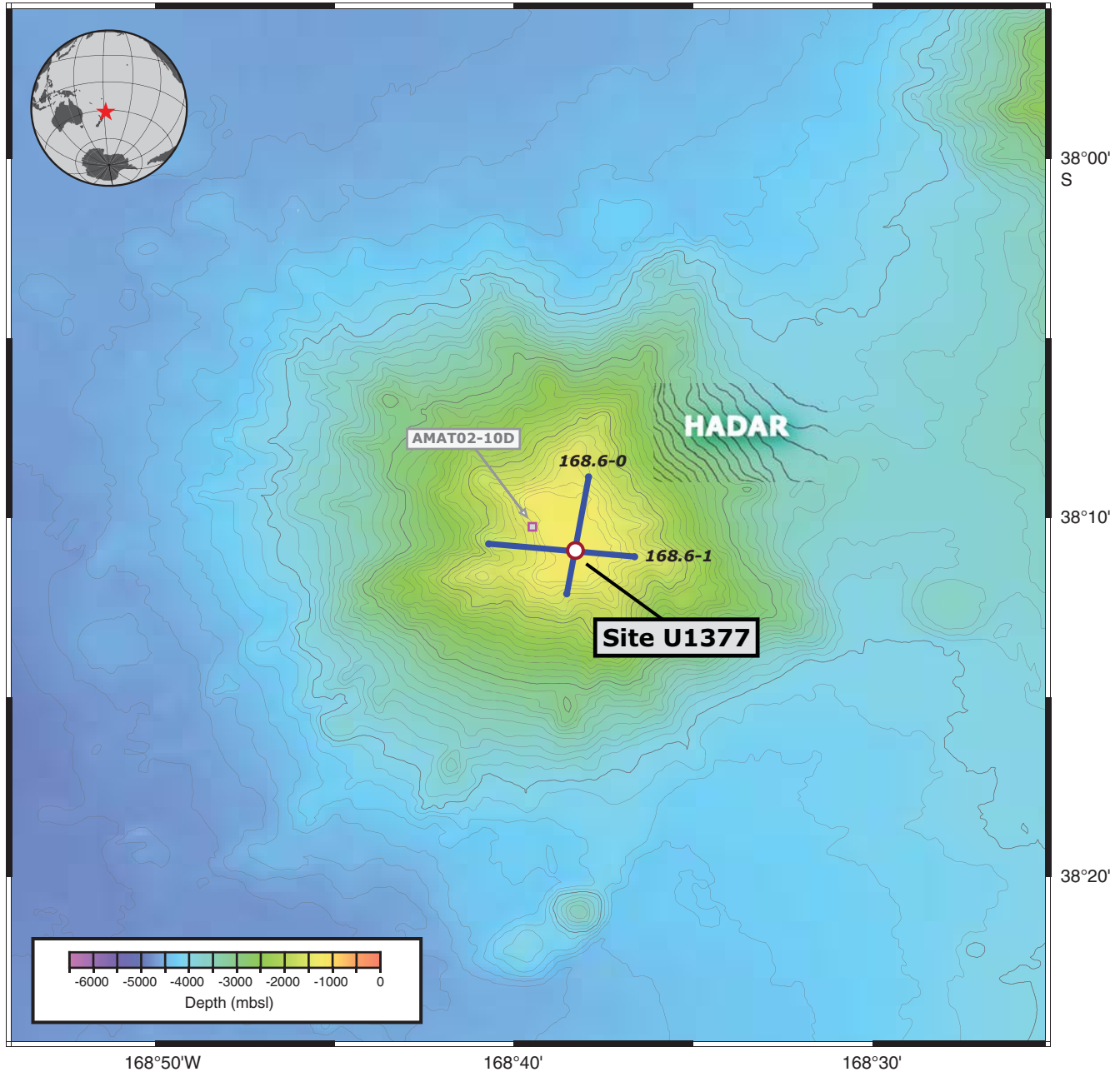






**Figure F4.** Close-up photographs of representative lithologies, Site U1377. **A.** Foraminiferal limestone with (1) ferromanganese-phosphorous encrustation in Unit II of Hole U1377A (interval 330-U1377A-2R-1A, 0–17 cm). **B.** Pale yellowish nannofossil foraminiferal ooze in Unit I of Hole U1377B (interval 330-U1377B-1R-1A, 10–30 cm). **C.** Multicolor basalt conglomerate with (1) ferromanganese encrustations in Unit II of Hole U1377B (interval 330-U1377B-1R-2A, 0–21.5 cm). Intercobble spaces are filled with bioturbated multicolor foraminiferal limestone. Also shown is (2) a geopetal structure defined by infilling of foraminiferal limestone and a void. **D.** Sediment pieces in ghost core in Hole U1377B (interval 330-U1377B-3G-1A, 13–36.5 cm). Upper four pieces are composed of foraminiferal limestone with ferromanganese encrustations. Lowermost piece (Piece 7) contains several lithologies: (1) grayish foraminiferal limestone with basalt clasts, (2) ferromanganese crust with concentric layering, and (3) bioturbated foraminiferal limestone with rare shallow-marine bioclasts.

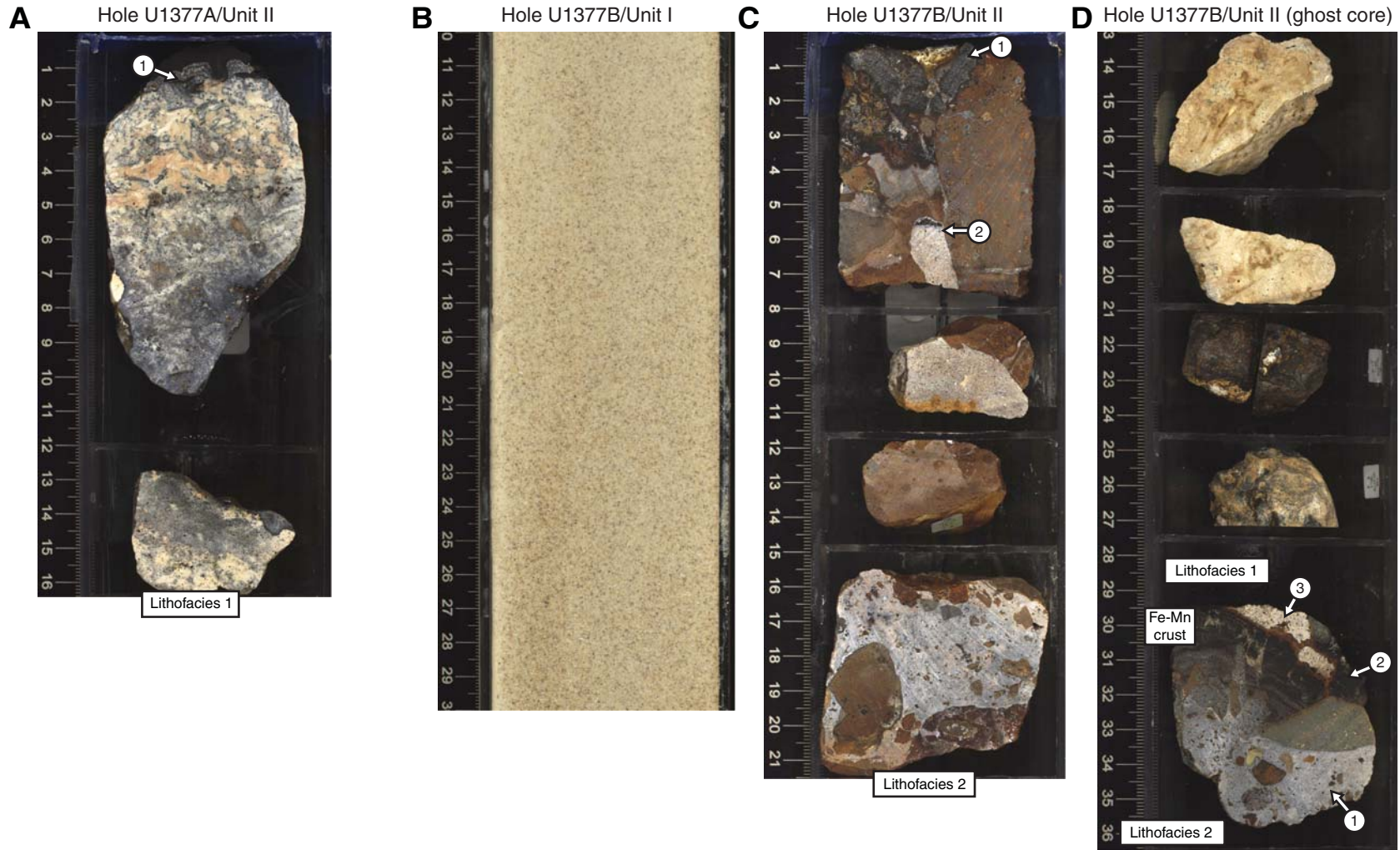




**Figure F5.** Calcareous nannofossil and planktonic foraminiferal biozonation, Holes U1377A and U1377B. Gray shaded areas indicate intervals barren of age-diagnostic calcareous microfossils. For legend of lithology patterns, see Figure F3.

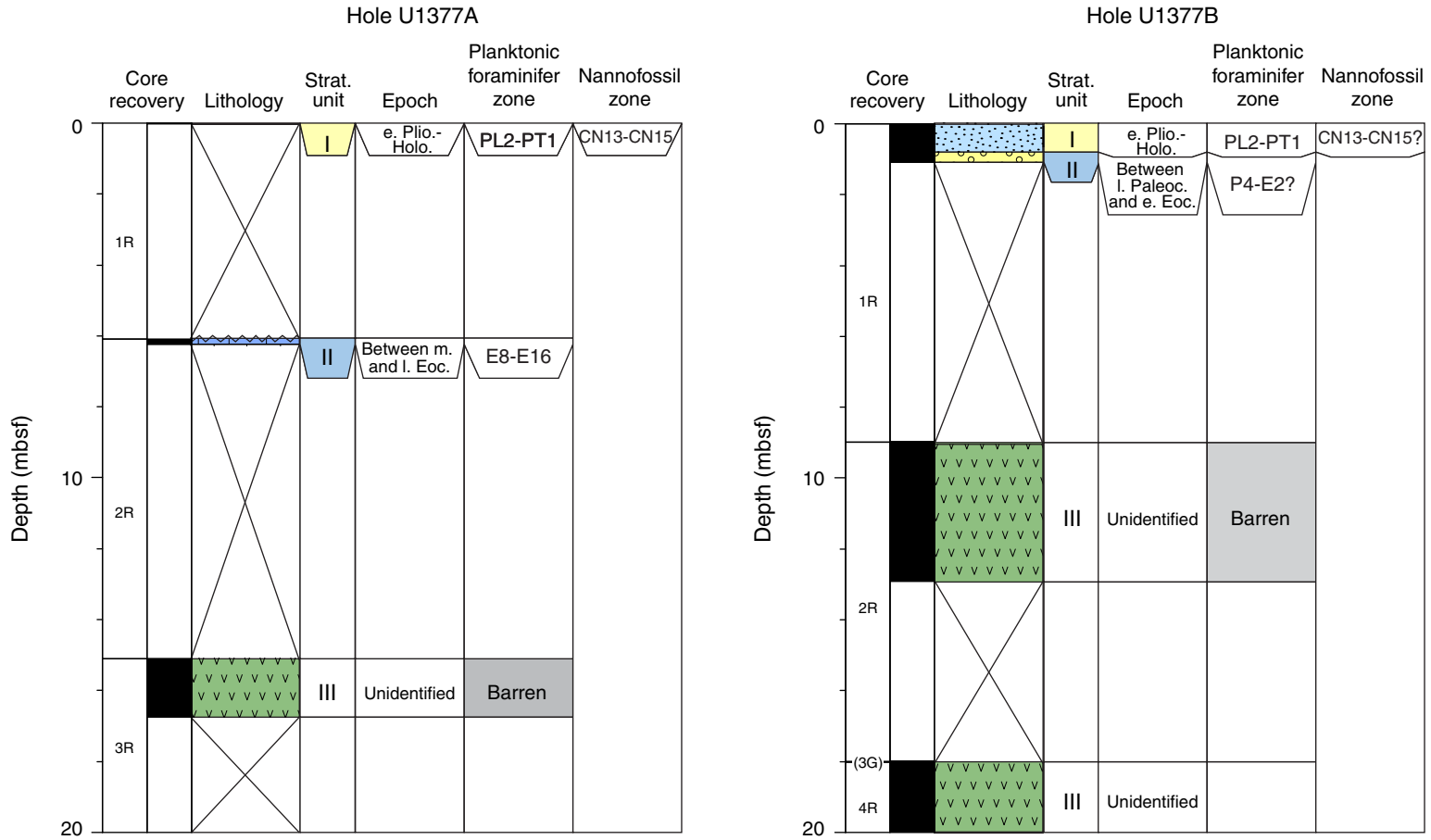


**Figure F6.** Thin section photomicrographs of planktonic foraminifers (Sample 330-U1377A-2R-1W, 15–17 cm; Thin Section 269). **A.** *Globigerinatheka* sp. **B.** *Acarinina* sp.

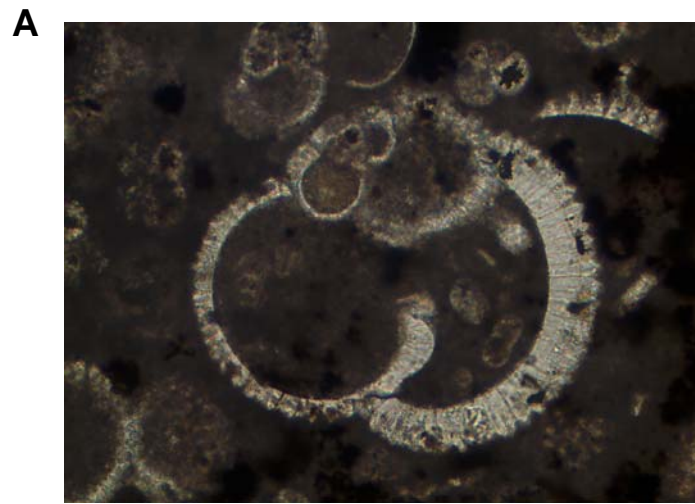




**Figure F7.** Thin section photomicrographs of planktonic foraminifers (Sample 330-U1377B-1R-2W, 8–12 cm; Thin Section 276). **A.** *Morozovella* sp. **B.** *Acarinina* sp.

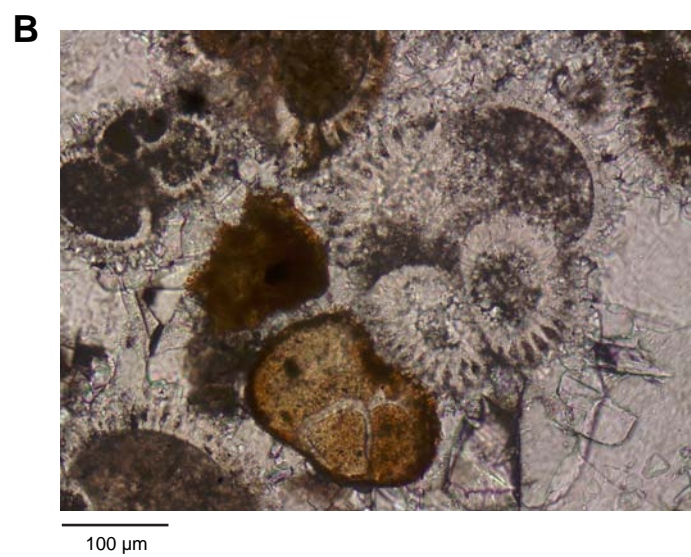




**Figure F8.** Stratigraphic summary of igneous rocks and lithologic features, Holes U1377A and U1377B. Core labeled “3G” is a ghost core retrieved while clearing Hole U1377B of debris and represents a cored interval of zero thickness.

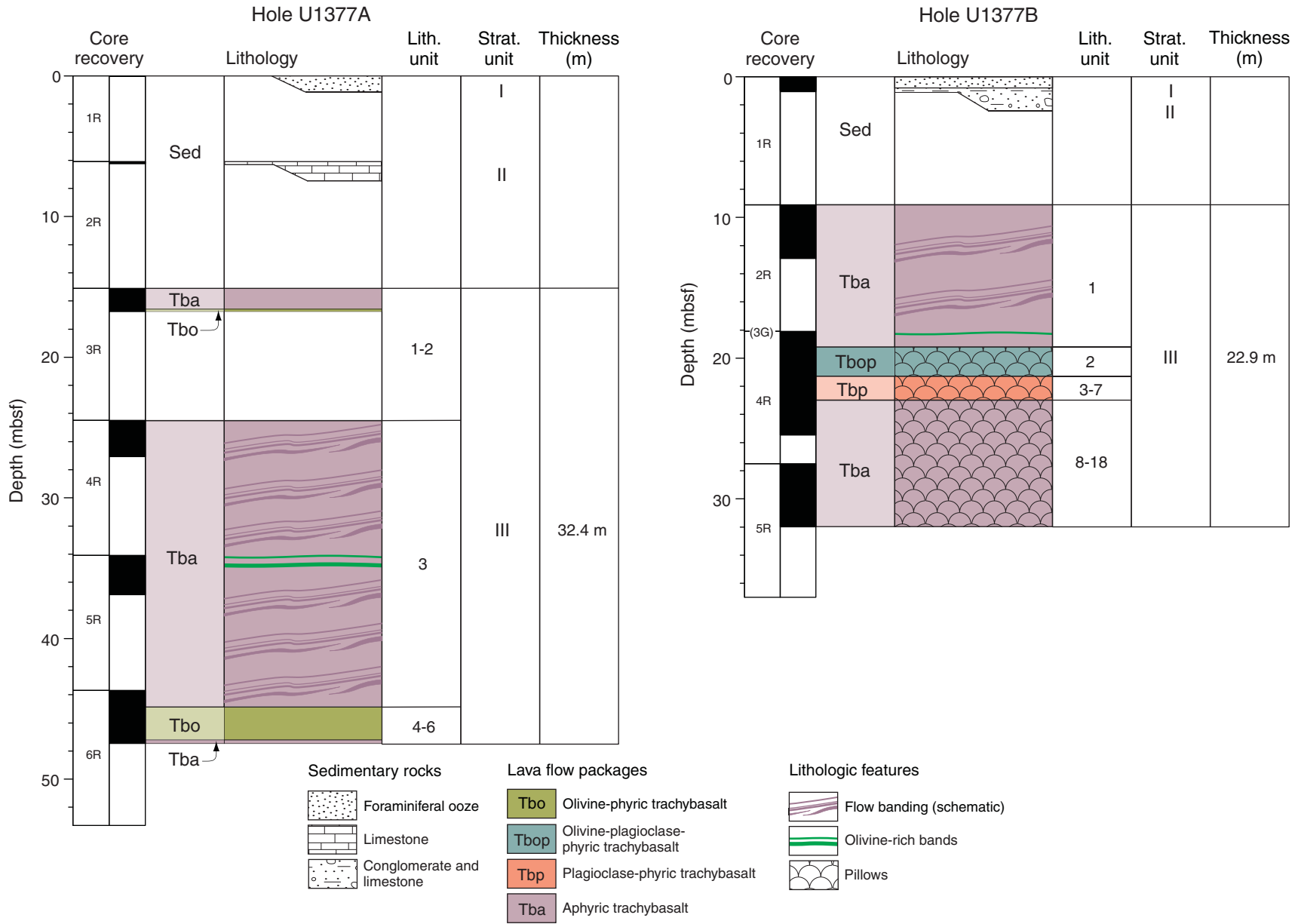


**Figure F9.** Scanned core photographs of flow banding in trachybasalt, Site U1377. **A.** Lithologic Unit 3 (interval 330-U1377A-4R-2A, 63–77 cm). **B.** Lithologic Unit 3 (interval 330-U1377A-6R-1A, 88–104 cm). Note the tendency of the rock to split along flow bands. **C.** Lithologic Unit 1 (interval 330-U1377B-2R-2A, 77–93.5 cm).

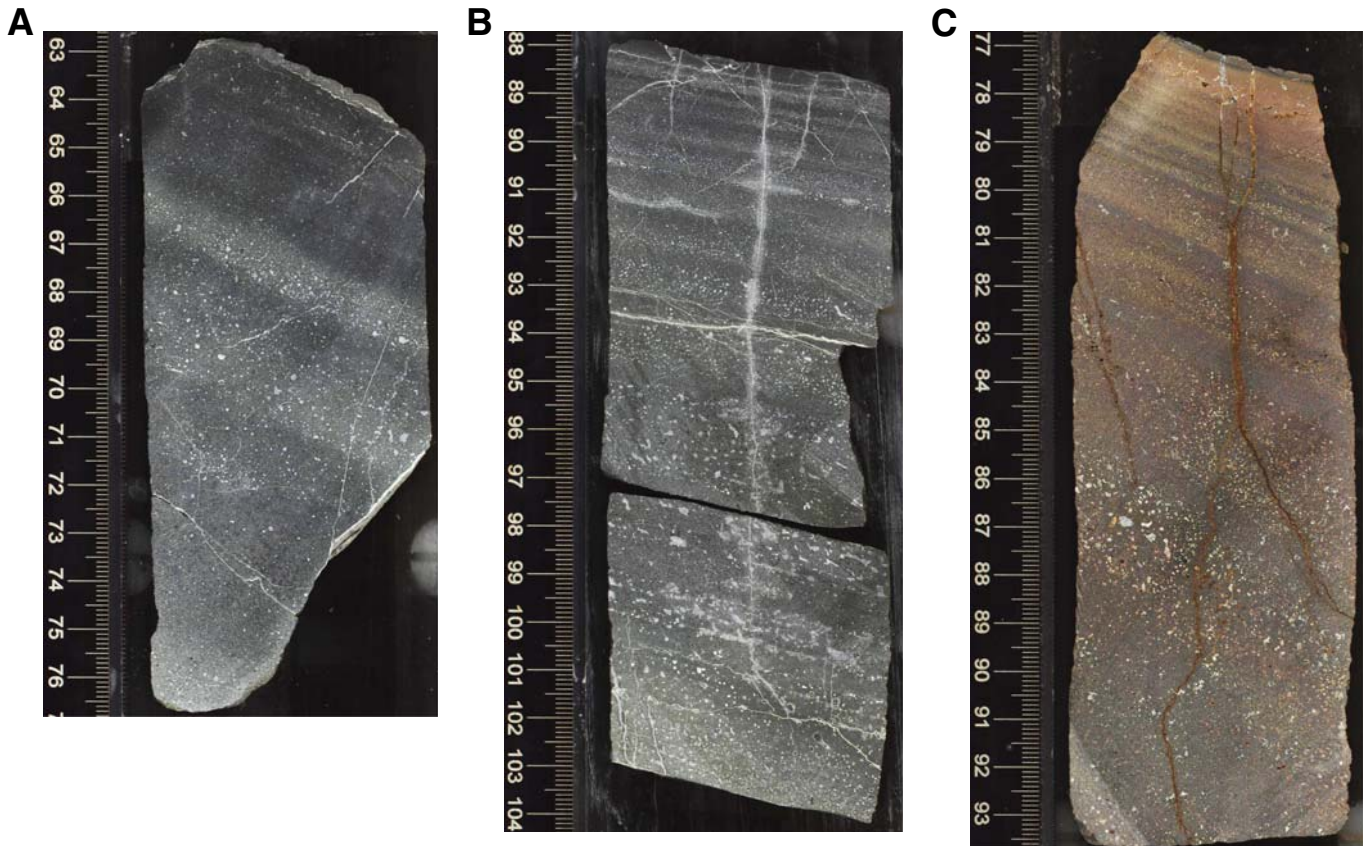


**Figure F10.** (A) Scanned core photograph and (B) sketched interpretation of contacts between lithologic Units 2, 3, and 4 in Hole U1377B (interval 330-U1377B-4R-3A, 102–140 cm). Lithologic Units 2 and 4 are pillows with glassy margins. Lithologic Unit 3 also has glassy margins and appears to have intruded into the space between lithologic Units 2 and 4. Units highlighted in B are colored according to lithology, as in the stratigraphic column in Figure F8.

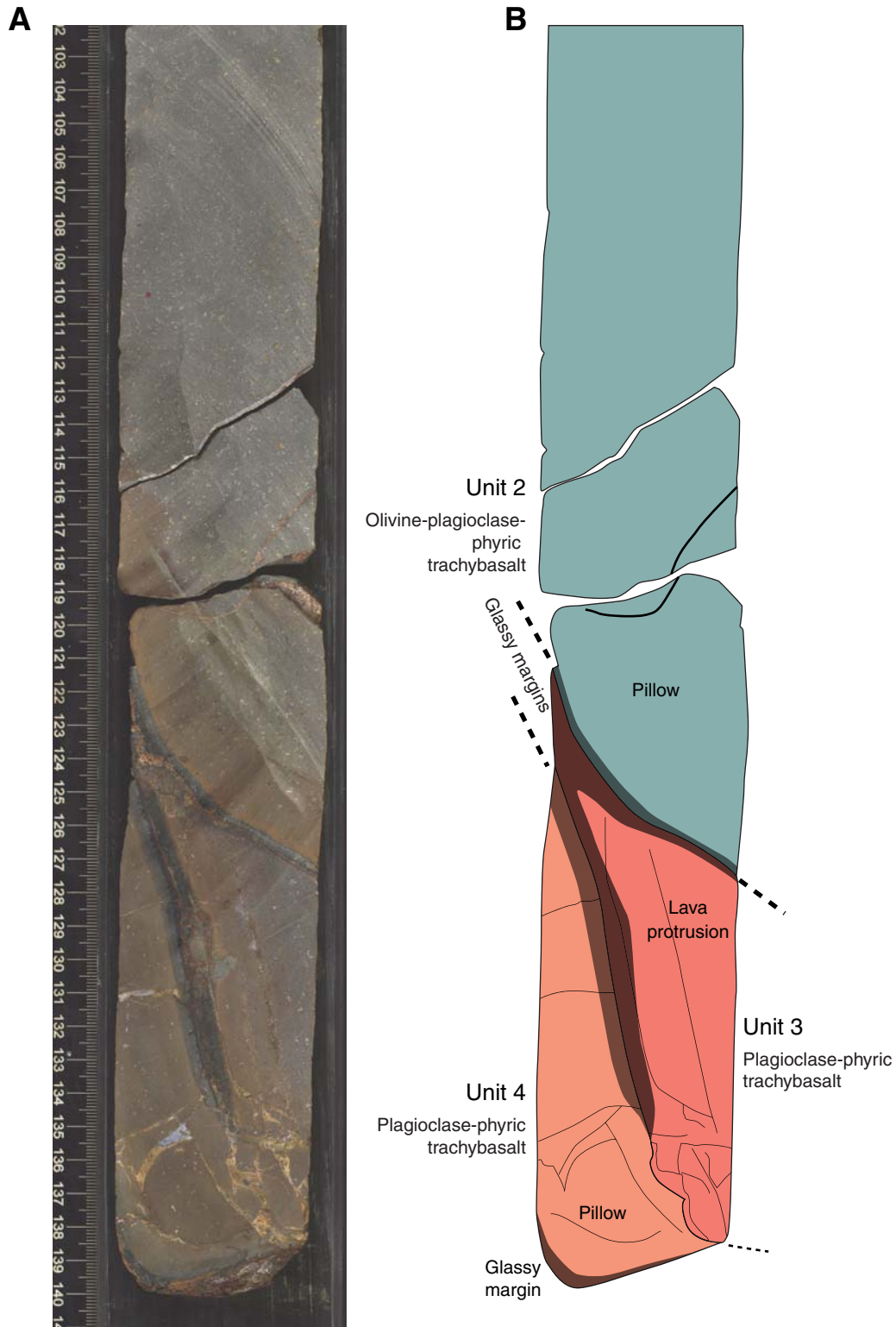


**Figure F11.** (A) Core photograph (wet) and (B) sketched interpretation showing relationships between lithologic Units 7, 8, and 9 (interval 330-U1377B-4R-5W, 1–34 cm). Lithologic Unit 9 appears to have intruded into breccia (Unit 7) to form a mixed zone (Unit 8), the intrusive matrix of which is glassy in its upper part. Part of the space between clasts was originally empty and is now filled with carbonate. Units highlighted in B are colored according to lithology, as in the stratigraphic column in Figure F8.

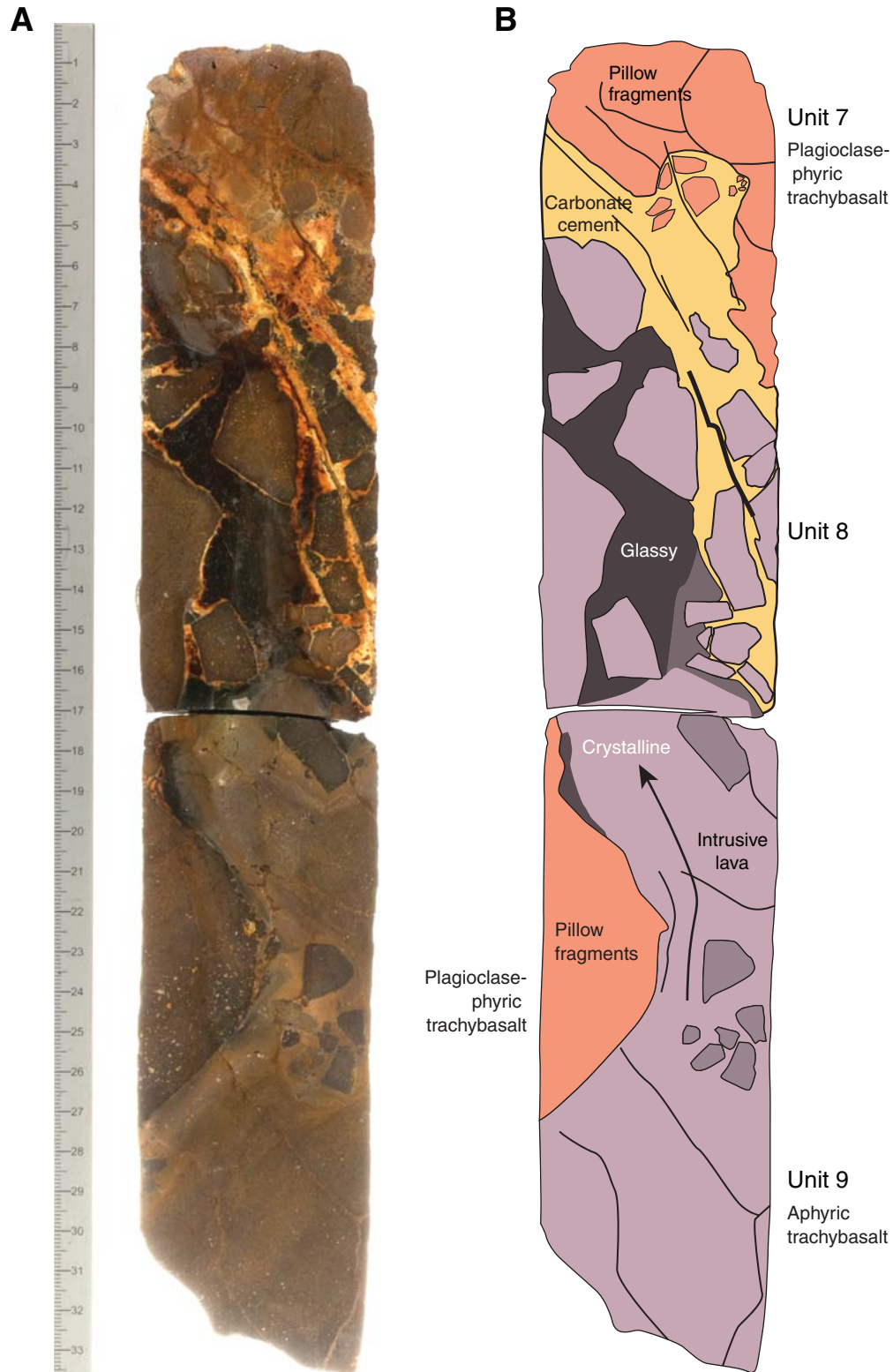


**Figure F12.** (A) Core photograph (wet) and (B) sketched interpretation of glassy protrusion from lithologic Unit 17 into Unit 16 (interval 330-U1377B-5R-2W, 94.5–124 cm). Units highlighted in B are colored according to lithology, as in the stratigraphic column in Figure F8.

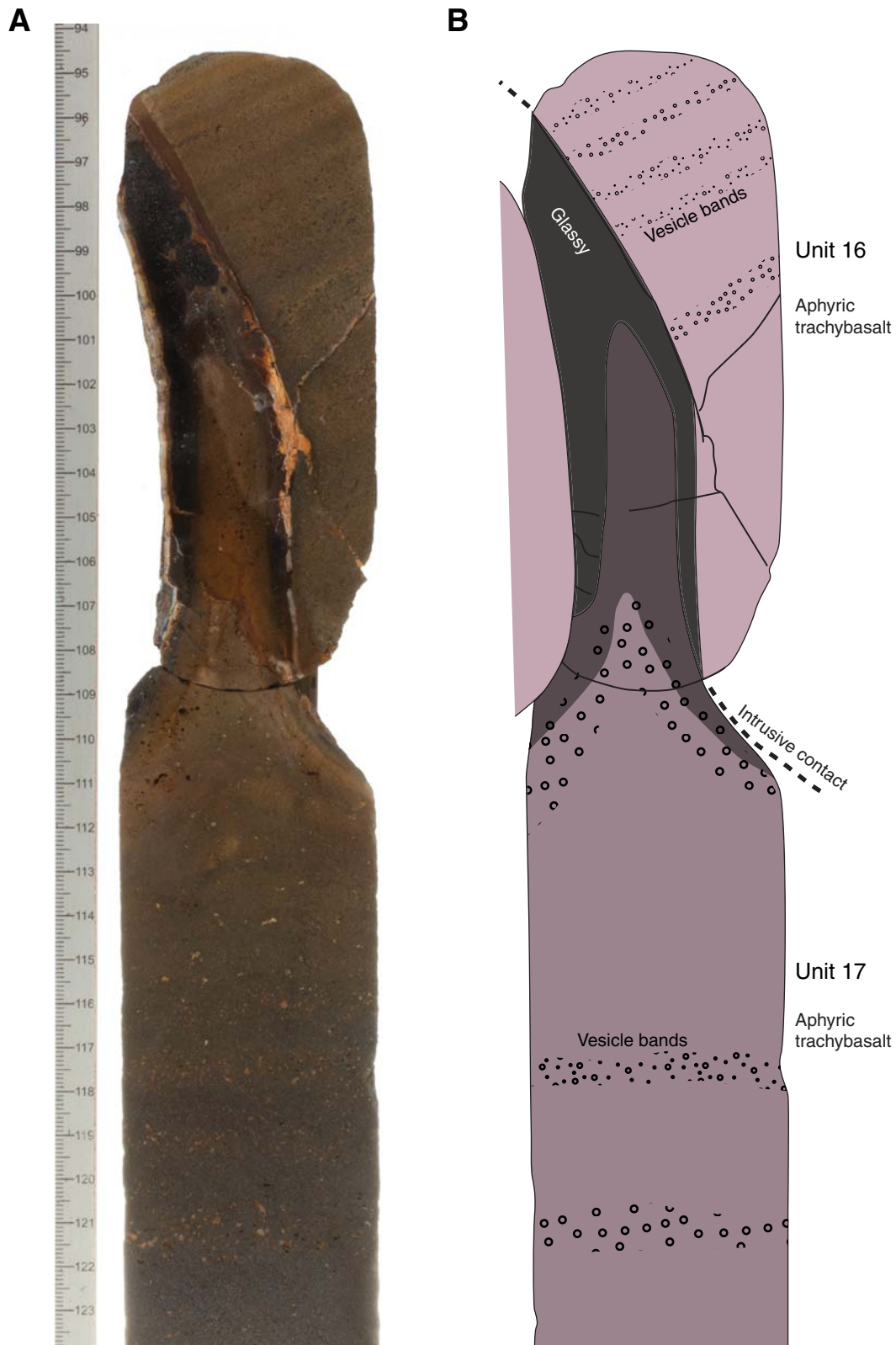


**Figure F13.** Plot of downhole distribution of main alteration colors representing overall color and alteration intensity of each lithologic unit (units defined by the igneous petrology group). Circles are located at center depth for each unit. For some units, especially those where volcanic clasts are surrounded by a volcanic matrix, the color of both clasts and matrix is reported. Gray shading represents sedimentary units.

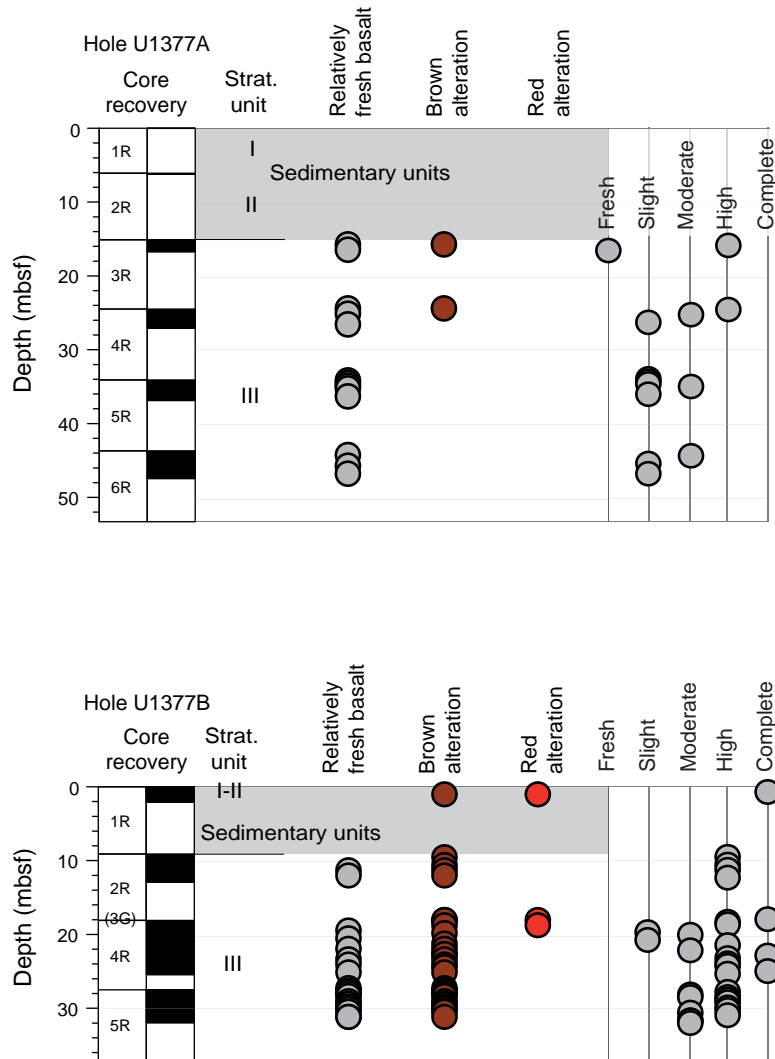


**Figure F14.** Plot of downhole distribution of secondary minerals after olivine for each alteration interval defined by the alteration petrology group. Symbols are located at center depth for each interval. Gray shading represents sedimentary units.

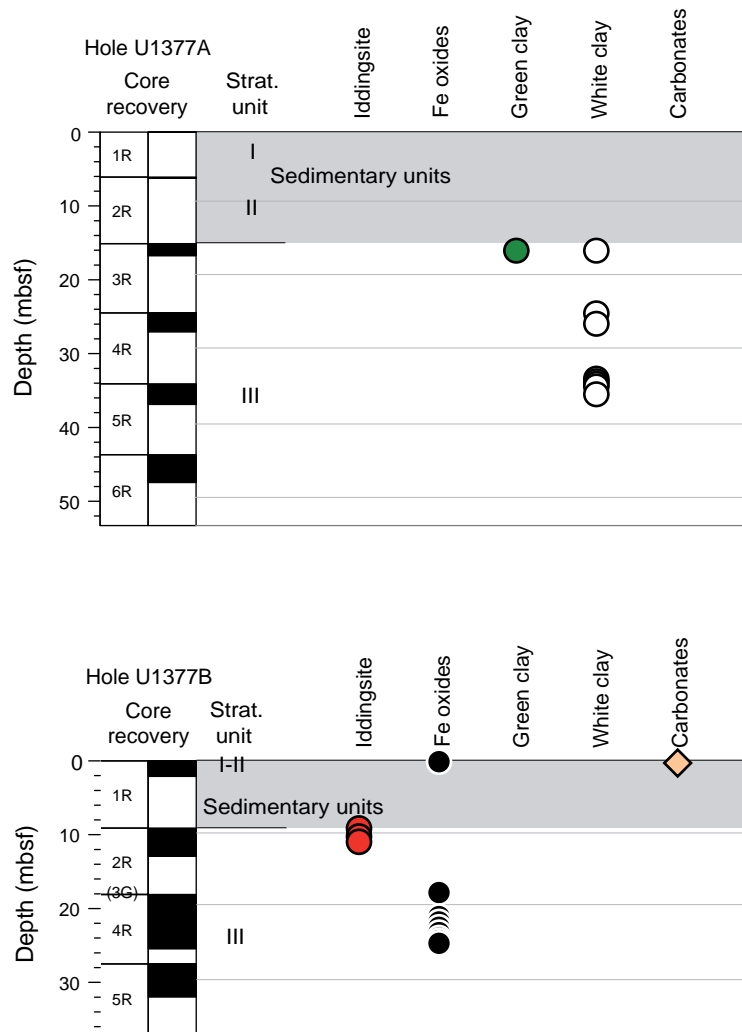




**Figure F15.** X-ray diffraction spectra and associated core photographs (analyzed zones are highlighted with red circle). **A.** Millimeter-thick vein filled with ankerite, Mg calcite, and siderite (Sample 330-U1377A-5R-2, 45–47 cm). **B.** Vesicle filled with Mg calcite and siderite (Sample 330-U1377A-6R2, 25–27 cm).

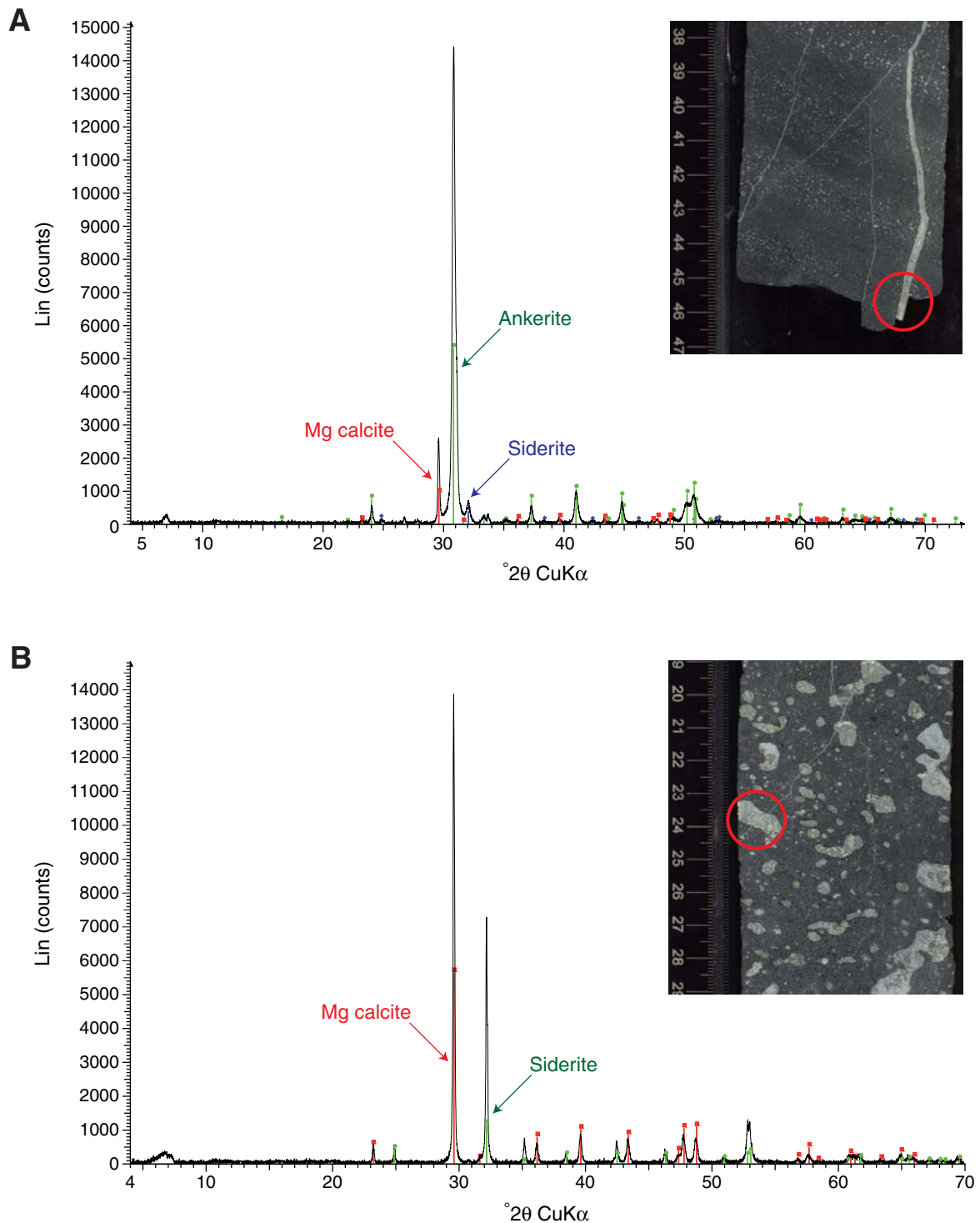


**Figure F16.** Thin section photomicrographs of vesicles and vein. **A.** Vesicles filled with thin layer of brown clay at rim and later by white clay and carbonates (in sparsely olivine-phyric lava lobe; Sample 330-U1377A-6R-2, 13–15 cm; Thin Section 274; crossed polars). **B.** Vesicles filled with carbonates (calcite and siderite; left) or different layers of brown and white clays (right) (in moderately olivine-phyric lava lobe; Sample 330-U1377A-6R-2, 64–66 cm; Thin Section 275; plane-polarized light). **C, D.** Vein filled with mix of clay minerals, Fe oxyhydroxides, and goethite (aphyric basalt lava body or intrusive sheet; Sample 330-U1377A-3R-1, 68–70 cm; Thin Section 270): (C) plane-polarized light, (D) reflected light.

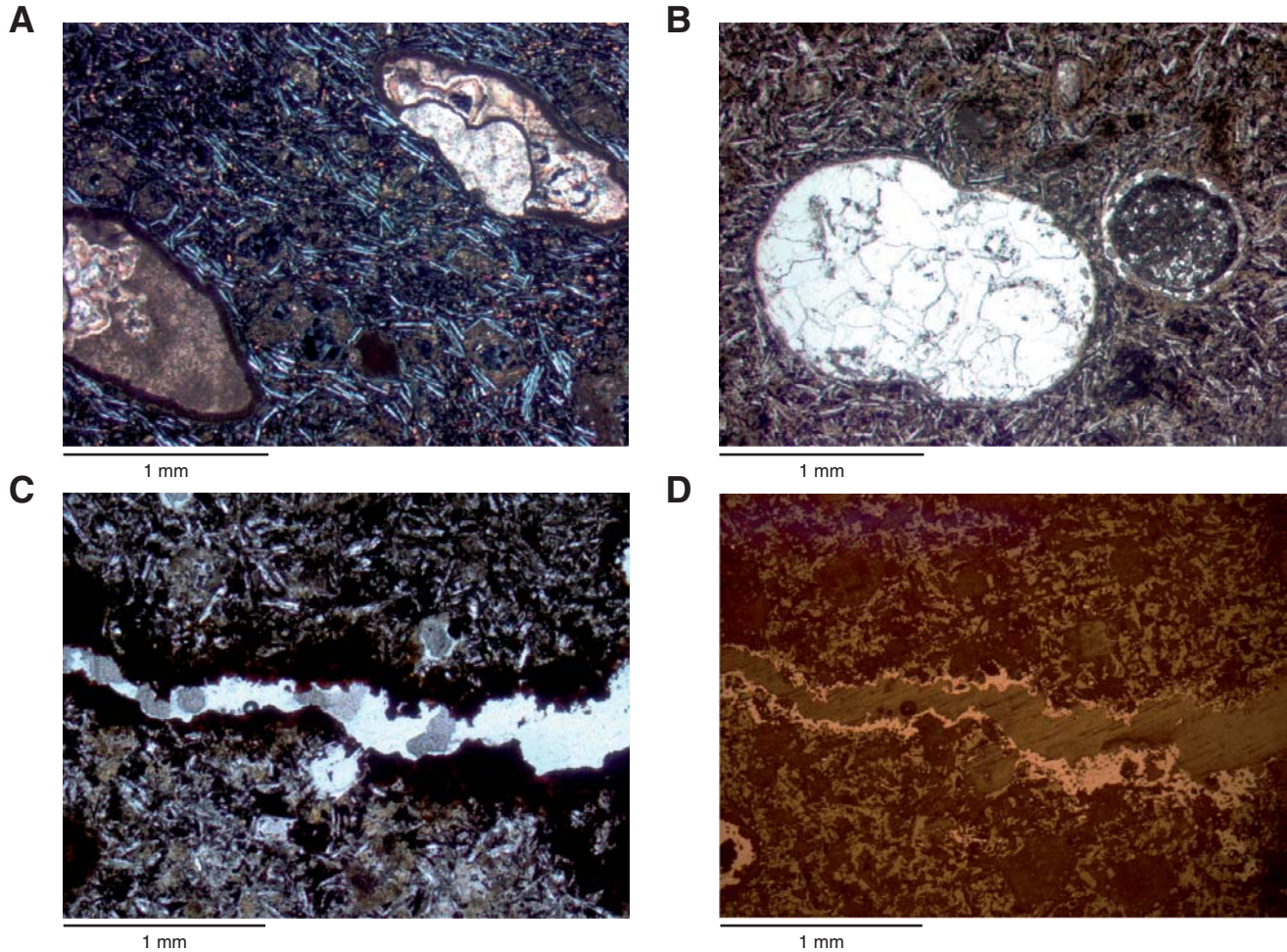


**Figure F17.** Plot of downhole distribution of alteration colors and groundmass alteration for each alteration interval defined by the alteration petrology group. Circles are located at center depth for each interval. Gray shading represents sedimentary units.

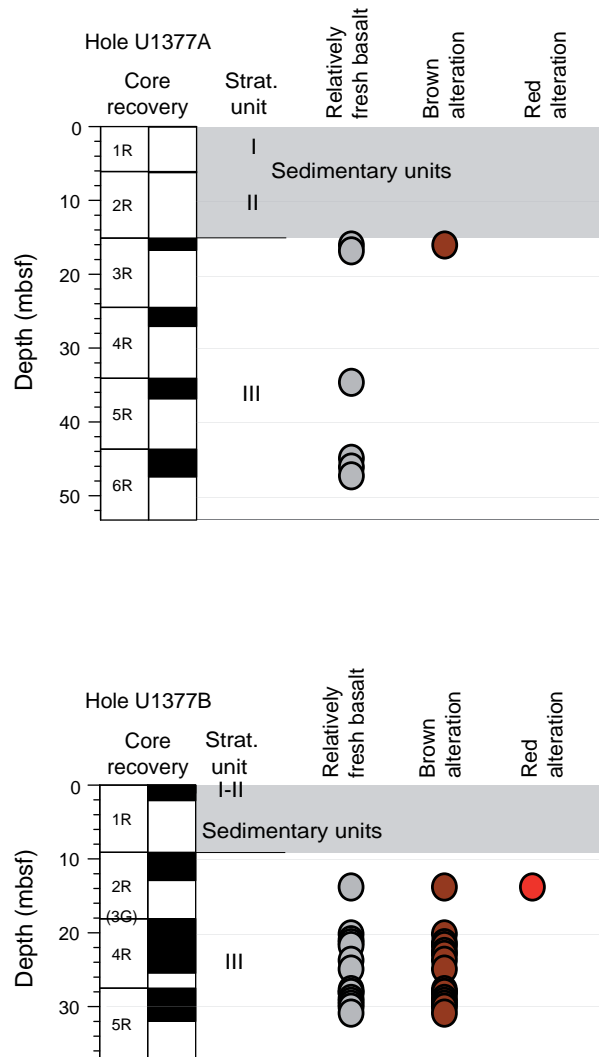


**Figure F18.** Plot of downhole distribution of secondary minerals infilling vesicles for each alteration interval defined by the alteration petrology group. Symbols are located at center depth for each interval. Gray shading represents sedimentary units.

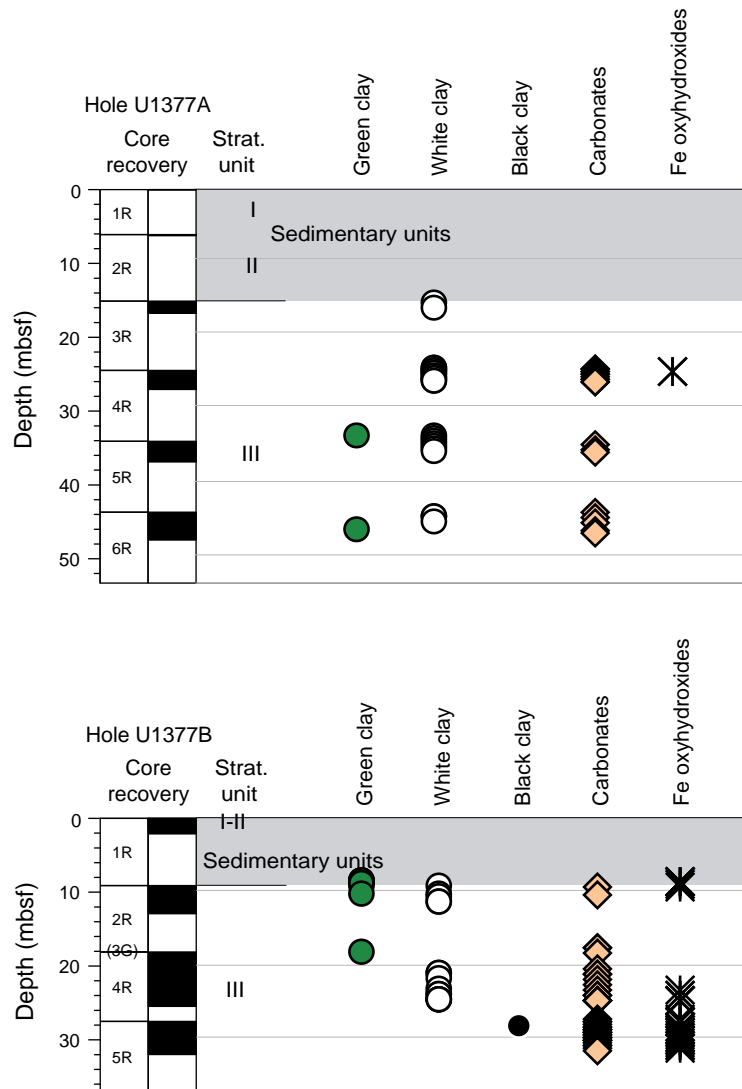


**Figure F19.** Plot of downhole distribution of vein minerals for each alteration interval defined by the alteration petrology group. Symbols are located at center depth for each interval. Gray shading represents sedimentary units.

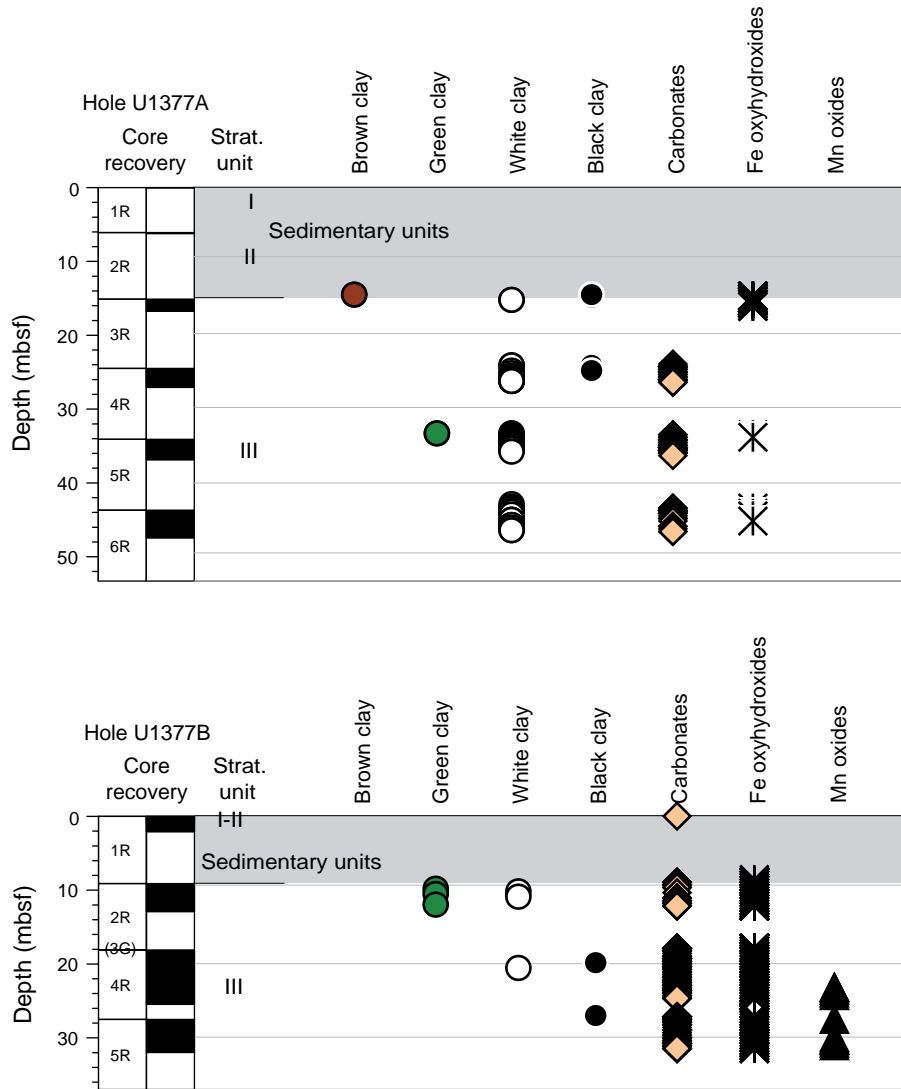


**Figure F20.** Close-up photographs of vesicles in hand specimens. Core surfaces were photographed dry. Arrows point toward top of core. **A.** Vesicles in aphyric to highly olivine-phyric basalt (interval 330-U1377A-4R-1, 50–60 cm). Vesicles are mainly filled with carbonates (calcite and siderite) and minor pyrite. **B.** Close-up photograph of the same rock, showing vesicle filled with pyrite along the margins and subsequently with carbonates (interval 330-U1377A-4R-1, 55–57 cm).

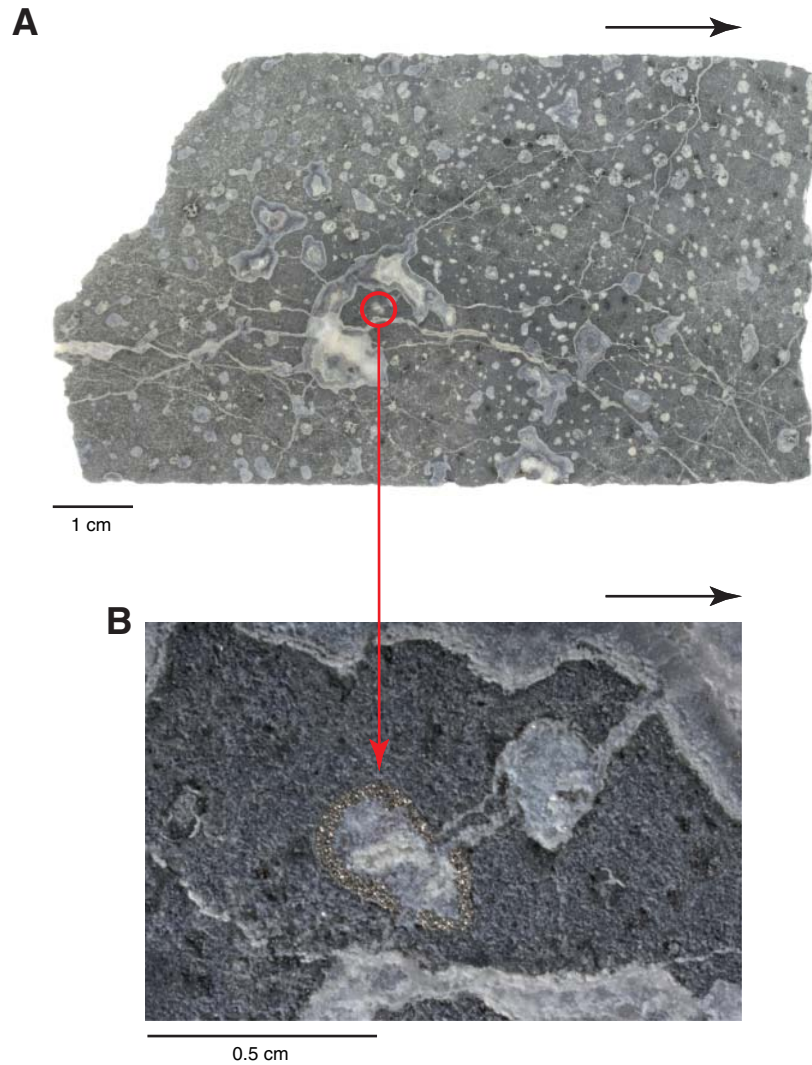


**Figure F21.** Number of structural features in (A) Hole U1377A and (B) Hole U1377B. The value  $N$  represents total number of features with individual row entries in the DESClogik database entry form. For veins, and especially vein networks, a single entry may comprise multiple features (e.g., 12 veinlets in a vein network). When multiple features are considered, there are 208 veins and 285 vein networks in Hole U1377A and 224 veins and 432 vein networks in Hole U1377B.

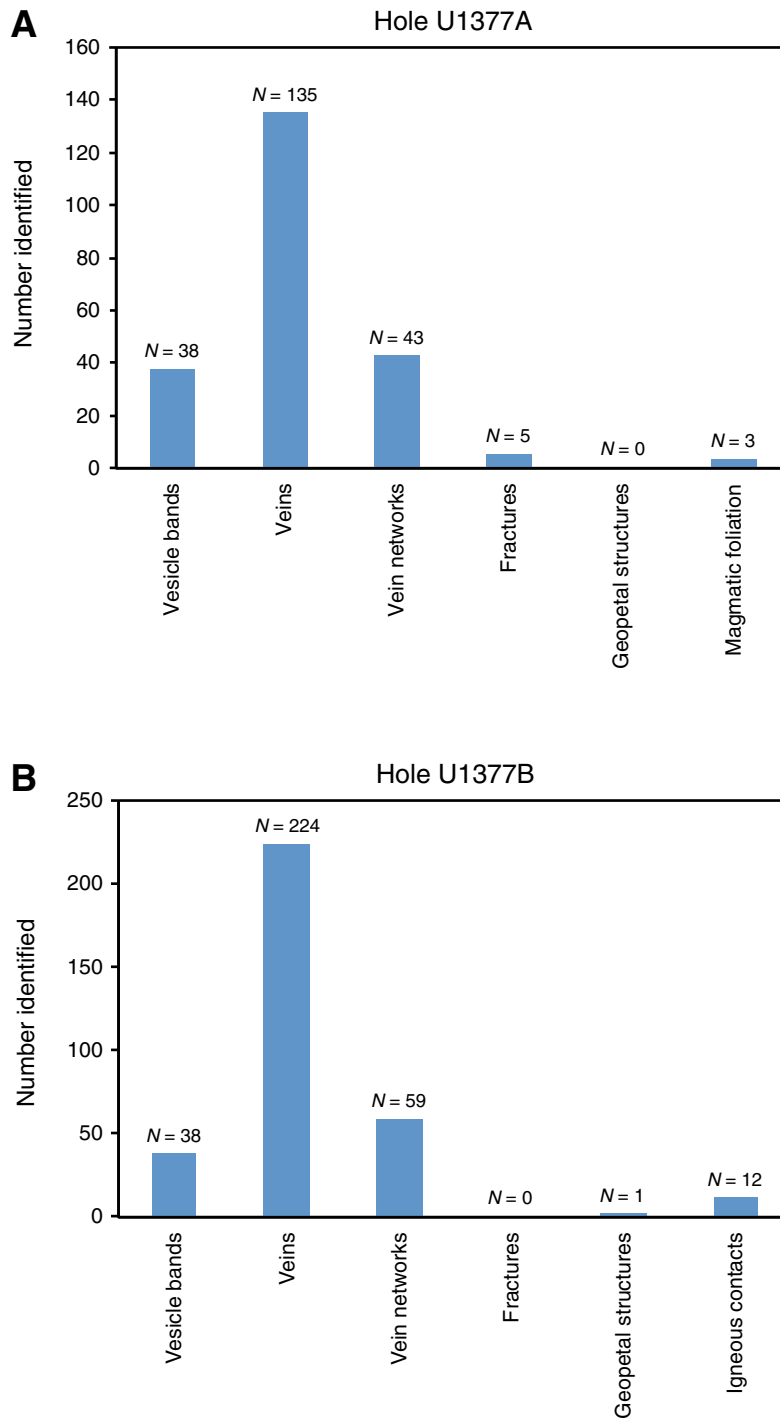


**Figure F22.** Distribution of veins and vein networks in (A) Hole U1377A and (B) Hole U1377B. Veins are abundant in all recovered basement units. For explanation of lithology symbols, see Figure F8. Core labeled “3G” (0–18.5 mbsf) is a ghost core retrieved while clearing the hole of debris (see “Operations”).

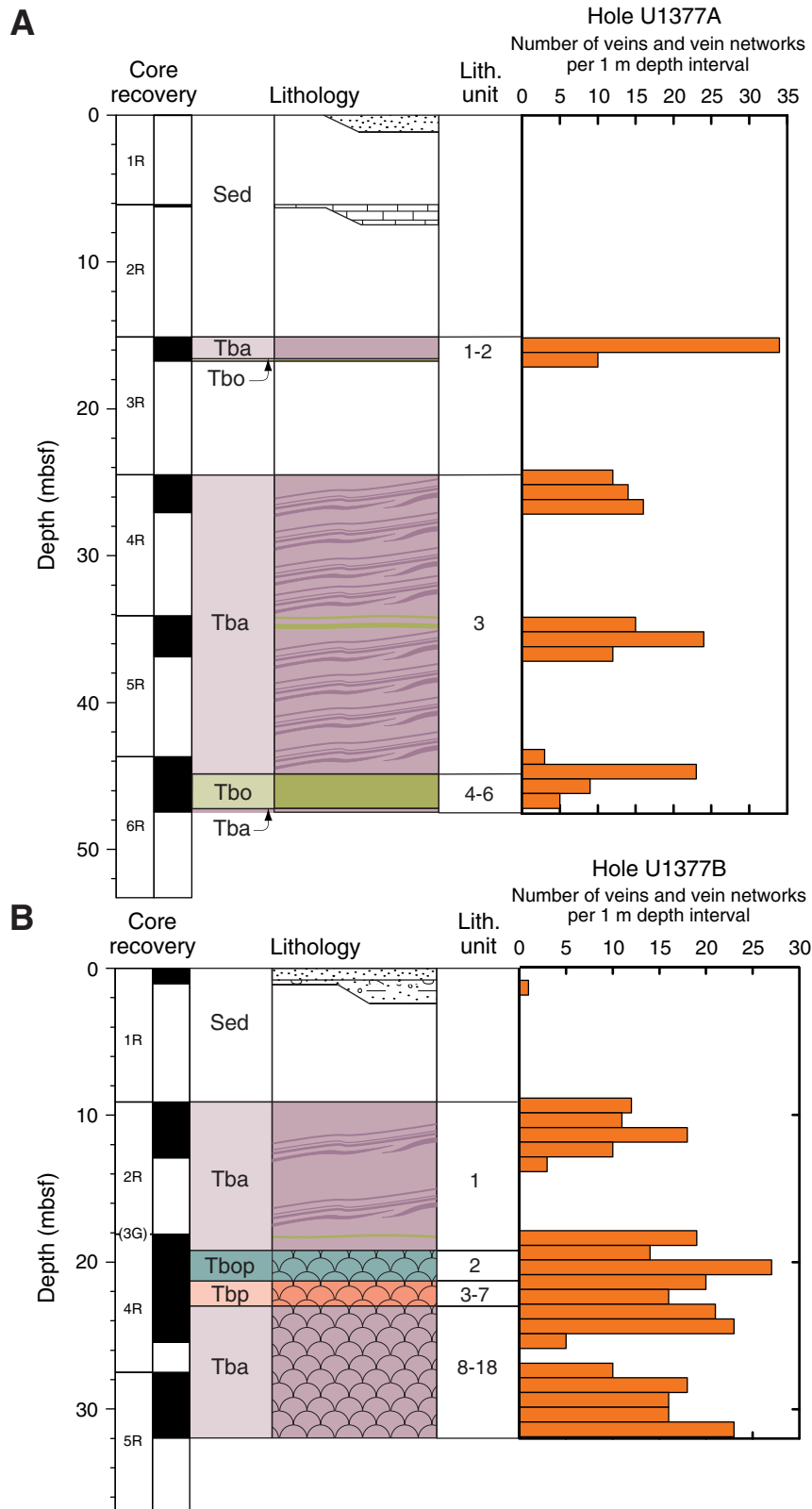






**Figure F23.** Dip angles of structures relative to core reference frame, Holes U1377A and U1377B. **A.** Veins and vein networks in Hole U1377A mostly have moderate to steep dips, with a maximum at 55°. **B.** Three fractures in aphyric lithologic Unit 3 also have moderate dips of 50°–60°. **C.** Vesicle bands and magmatic foliations in Hole U1377A are mostly subhorizontal (dips < 10°) or steeply dipping (~65°). **D.** Veins and vein networks in Hole U1377B also dominantly have steep dips, with a maximum at 55°. **E.** Dips for glassy chilled contacts in Hole U1377B range from 45° to 90°. **F.** Vesicle bands in Hole U1377B are mostly steeply dipping, with a maximum at 55°–60°.

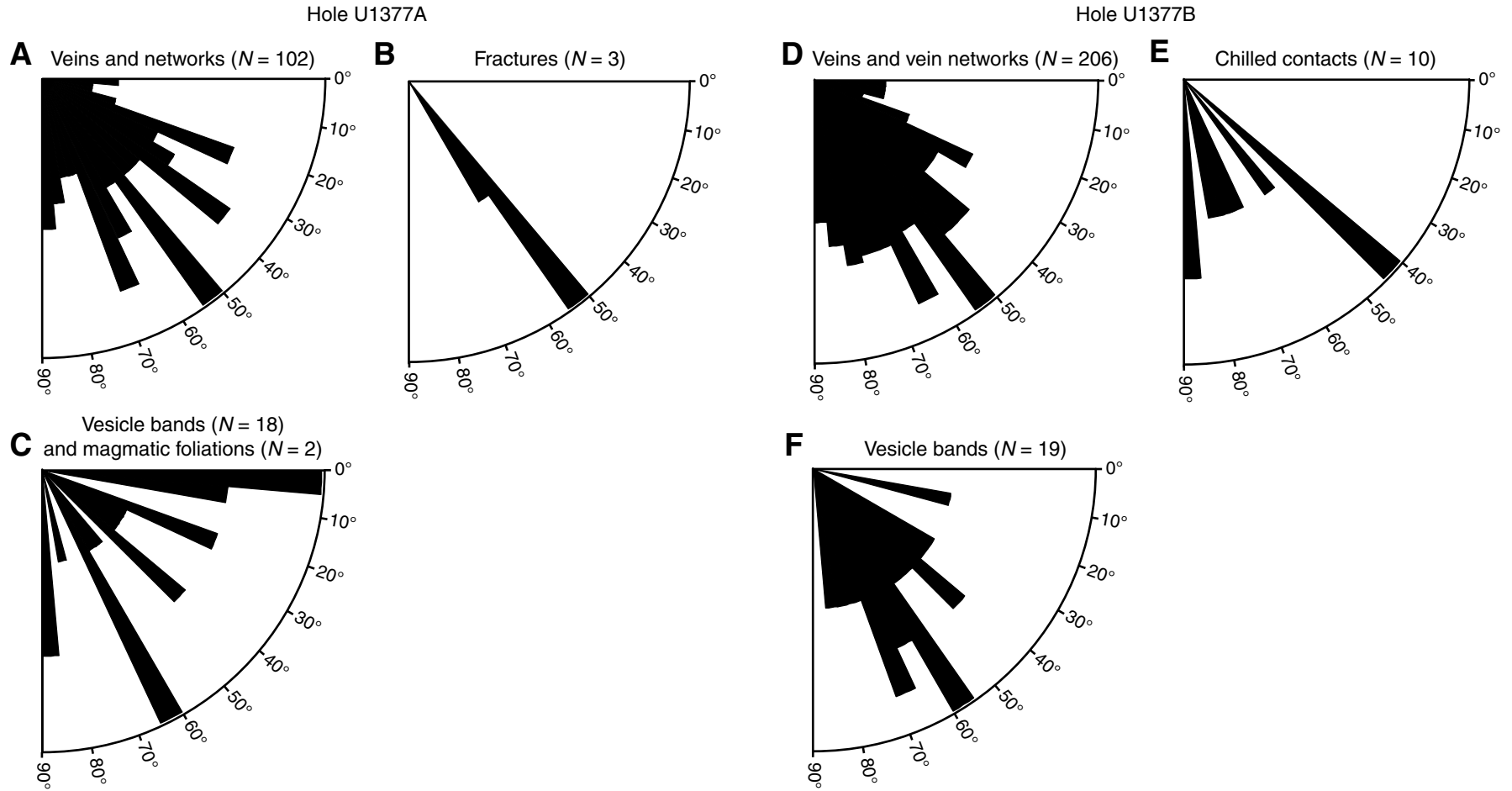


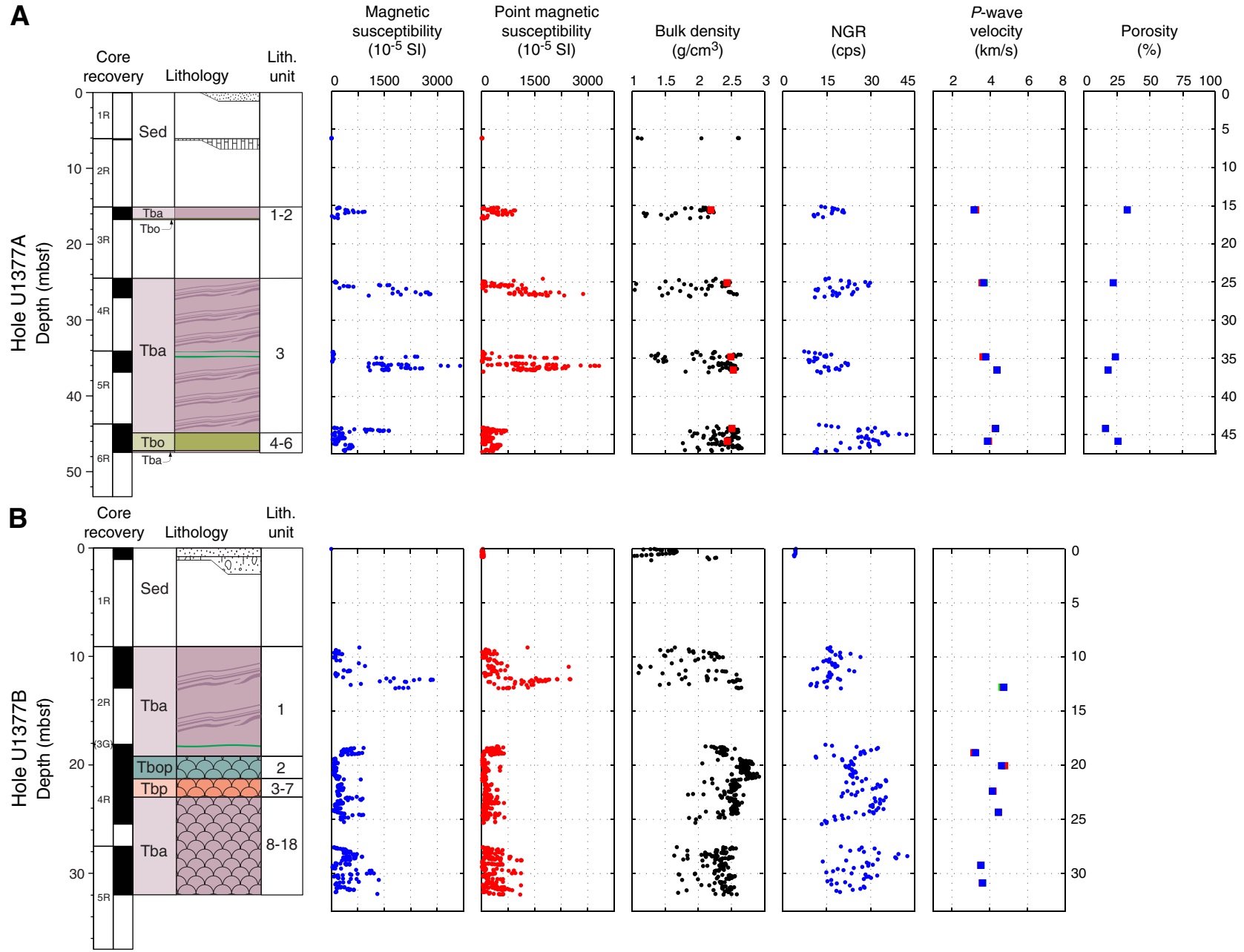
Figure F24. Core photograph of horizontal geopetal structure (interval 330-U1377A-1R-2A, 0–7.5 cm).



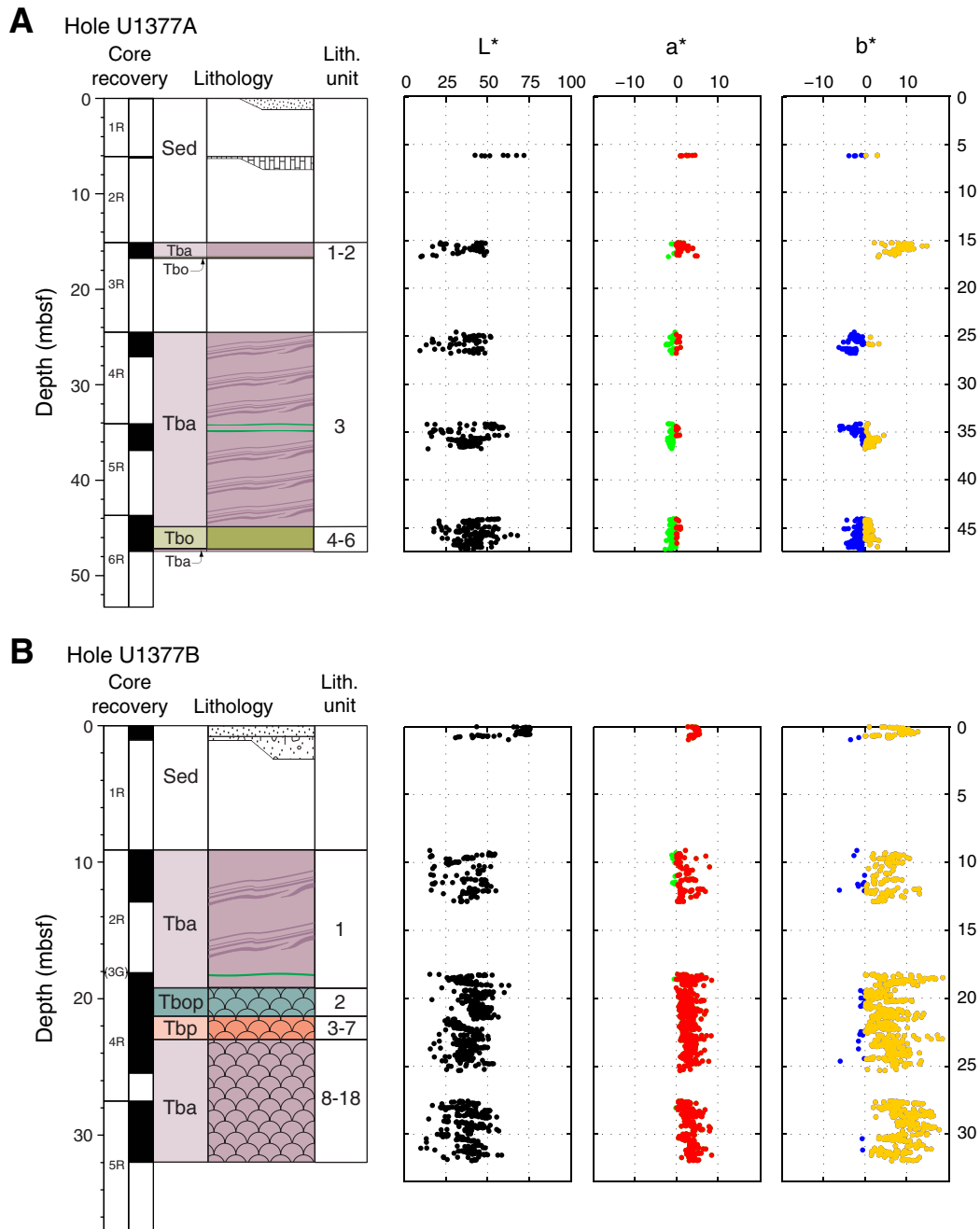
**Figure F25.** Depth profiles of physical property measurements, (A) Hole U1377A and (B) Hole U1377B. Stratigraphic columns for each hole are shown for reference. For explanation of stratigraphy, see Figure F8. The vertical scale for each hole is different to reflect the different levels of recovery. Bulk density: black dots = GRA bulk density, red squares = moisture and density Method C (MAD-C) measurements on discrete samples from Hole U1377A. *P*-wave velocity: blue = *x*-axis (normal to the split-core surface), red = *y*-axis (parallel to the split-core surface), green = *z*-axis (downcore). Porosity from measurements on discrete samples is shown for Hole U1377A only. NGR = natural gamma radiation. (Figure shown on next page.)



Figure F25 (continued). (Caption shown on previous page.)



**Figure F26.** Depth profile of color reflectance parameters  $L^*$ ,  $a^*$ , and  $b^*$ , (A) Hole U1377A and (B) Hole U1377B. The vertical scale for each hole is different to reflect the different levels of recovery. Higher  $L^*$  values indicate lighter colors.  $a^*$  = relative color position between red (positive) and green (negative),  $b^*$  = relative color position between yellow (positive) and blue (negative). Stratigraphic columns for each hole are shown for reference. For explanation of stratigraphy, see Figure F8.



**Figure F27.** Downhole plots of paleomagnetic data from archive-half cores, Hole U1377A and U1377B. **A.** Core recovery and observed stratigraphy (see Fig. F8 for explanation of patterns and abbreviations). **B.** Remanent intensity variations: purple = NRM intensities, black = intensities associated with principal component analysis (PCA) directions with misfits  $\leq 2.42$  (Hole U1377A) and  $\leq 1.89$  (Hole U1377B), gray = intensities associated with PCA directions with misfits  $> 2.42$  (Hole U1377A) and  $> 1.89$  (Hole U1377B). **C.** WRMSL magnetic susceptibility (see “Physical properties”). **D.** Inclination: red = PCA directions with misfits  $\leq 2.42$  (Hole U1377A) and  $\leq 1.89$  (Hole U1377B), pink = PCA directions with misfits  $> 2.42$  (Hole U1377A) and  $> 1.89$  (Hole U1377B). **E.** Median destructive field of the vector difference sum (MDF'), shown only for intervals with low misfits.

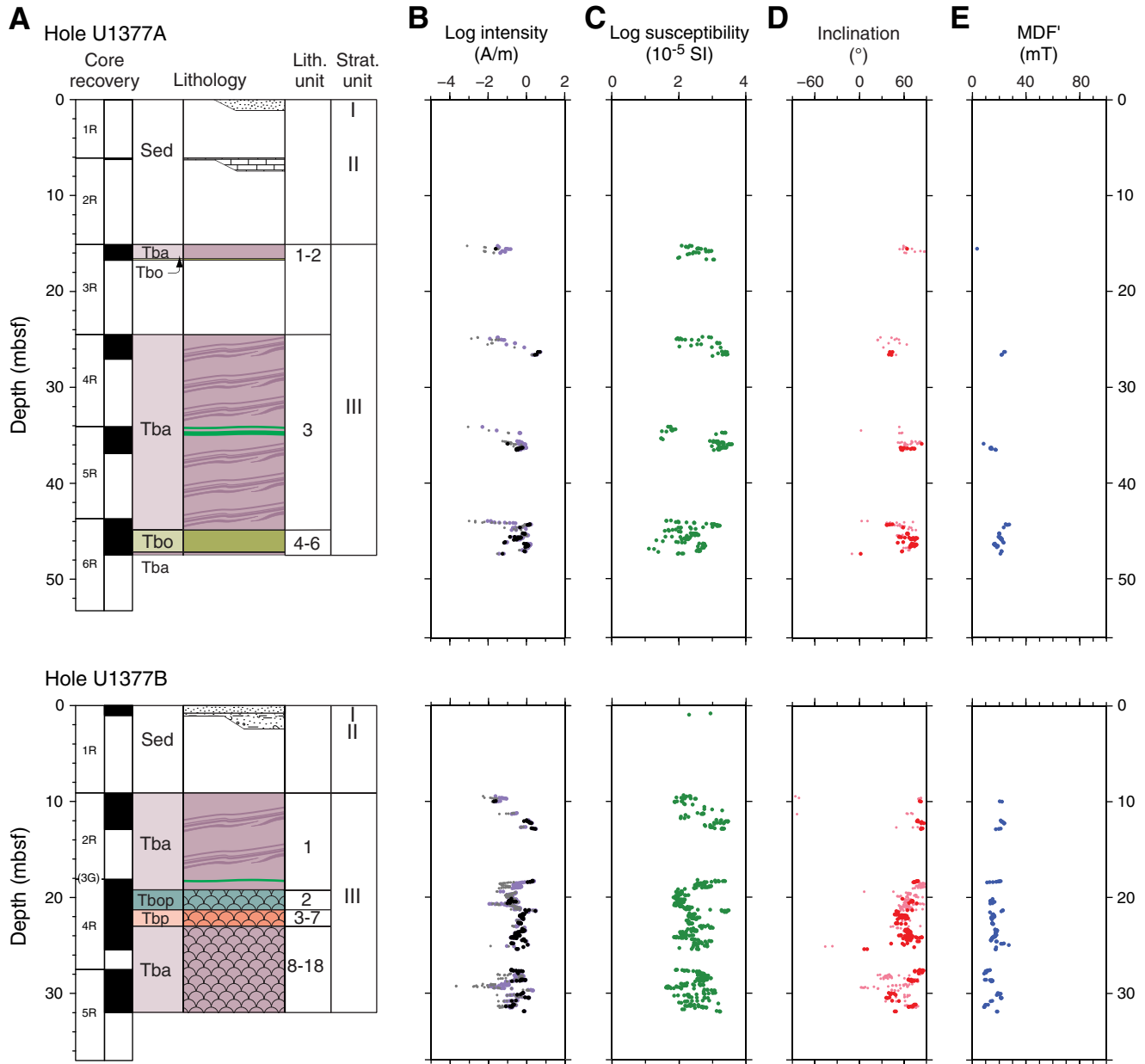


**Figure F28.** Log-log graph of natural remanent magnetization (NRM) intensity vs. Königsberger ratio ( $Q_n$ ) for discrete samples, Holes U1377A and U1377B.

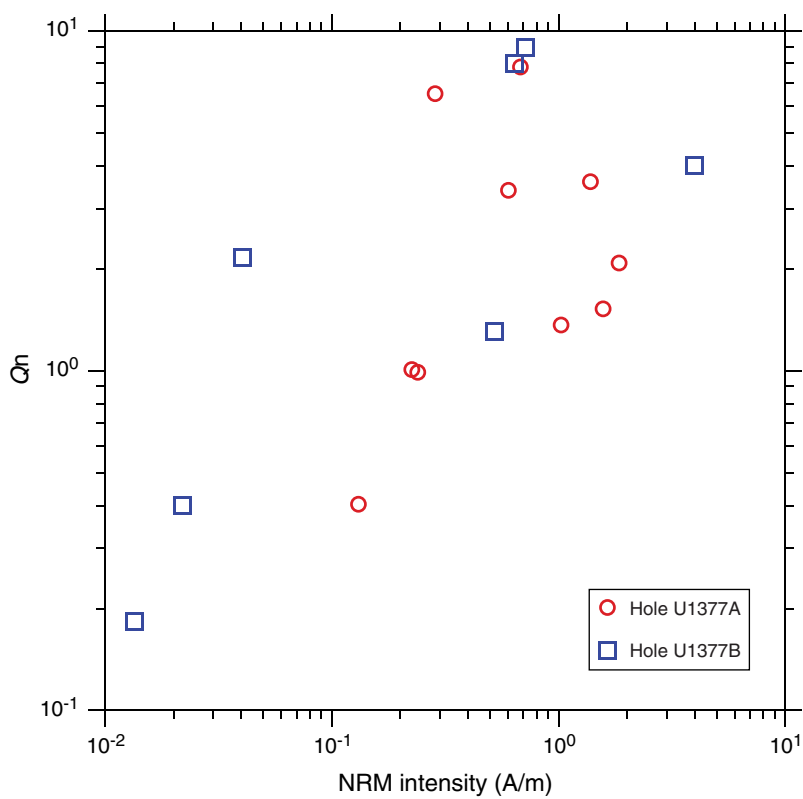


**Figure F29.** A–C. Representative Zijdeveld plots of stepwise AF and thermal demagnetization results from discrete samples, Hole U1377A. Solid circles = projections of vector endpoints onto horizontal plane, open circles = projections onto vertical plane. Red arrows = best-fitting principal component analysis direction. Gray boxes indicate thermal and AF demagnetization results from adjacent samples. NRM = natural remanent magnetization.

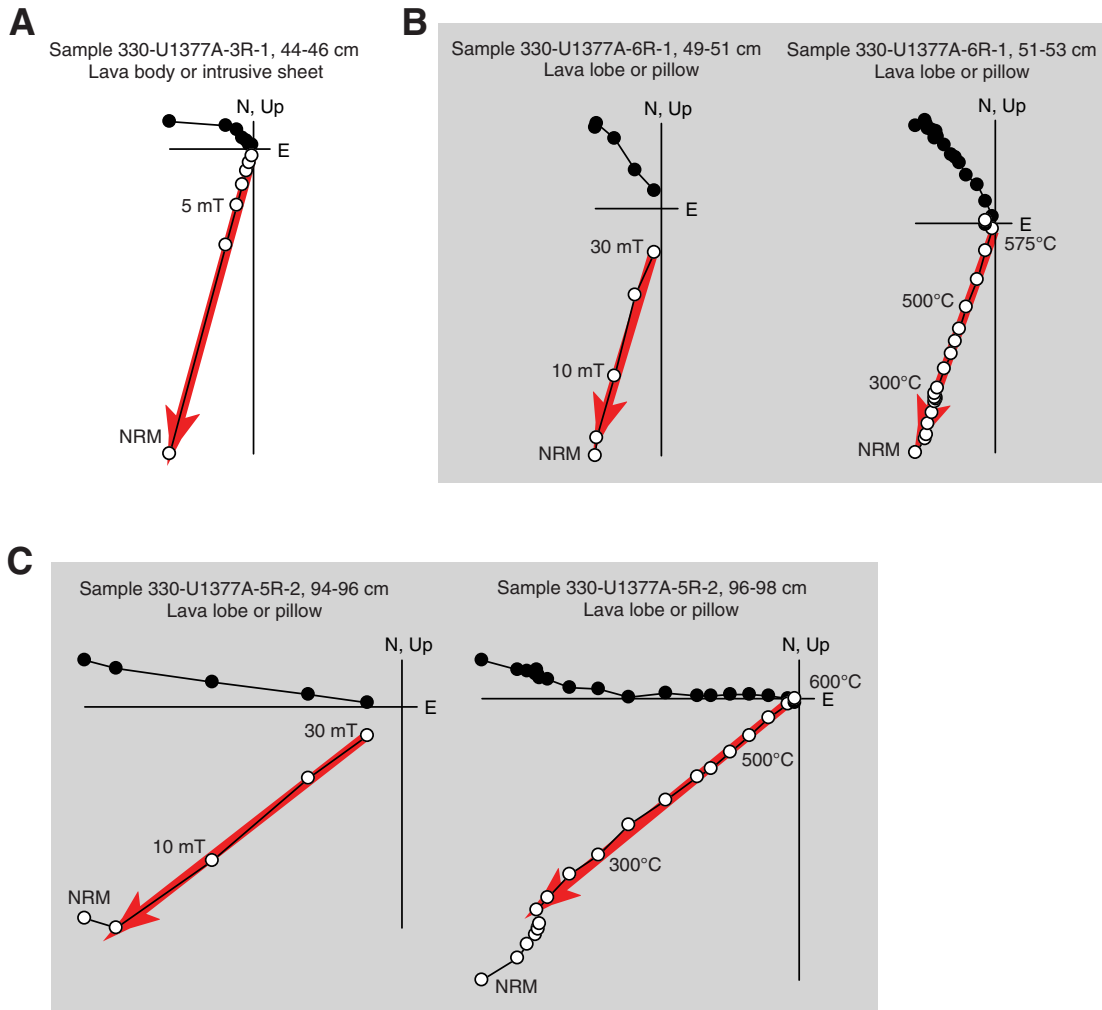




**Figure F30.** Downhole plots of inclination, Holes U1377A and U1377B. **A.** Core recovery and observed stratigraphy (see Fig. F8 for explanation of patterns and abbreviations). **B.** All downhole inclination data measured at 2 cm intervals on archive-half cores: red = principal component analysis (PCA) directions with misfits  $\leq 2.42$  (Hole U1377A) and  $\leq 1.89$  (Hole U1377B), pink = PCA directions with misfits  $> 2.42$  (Hole U1377A) and  $> 1.89$  (Hole U1377B). **C.** Average inclination for each lithologic unit (see “[Igneous petrology and volcanology](#)”), calculated using inclination-only statistics (Arason and Levi, 2010). **D.** Average inclination for each core piece longer than 9 cm, calculated using Fisher statistics. **E.** Average inclination for each lithologic unit, calculated using average piece directions displayed in D and inclination-only statistics. **F.** Characteristic remanent magnetization inclinations from discrete samples (from alternating-field [AF] or thermal demagnetization) with maximum angular deviation  $\leq 5^\circ$ . Shading scheme for C–F represents the ISCI for identifying distinct lava flow units, where the darkest shade of blue is the most confident and green is not applicable (NA; i.e., deposits cannot have retained their orientation since cooling). (Figure shown on next page.)



Figure F30 (continued). (Caption shown on previous page.)

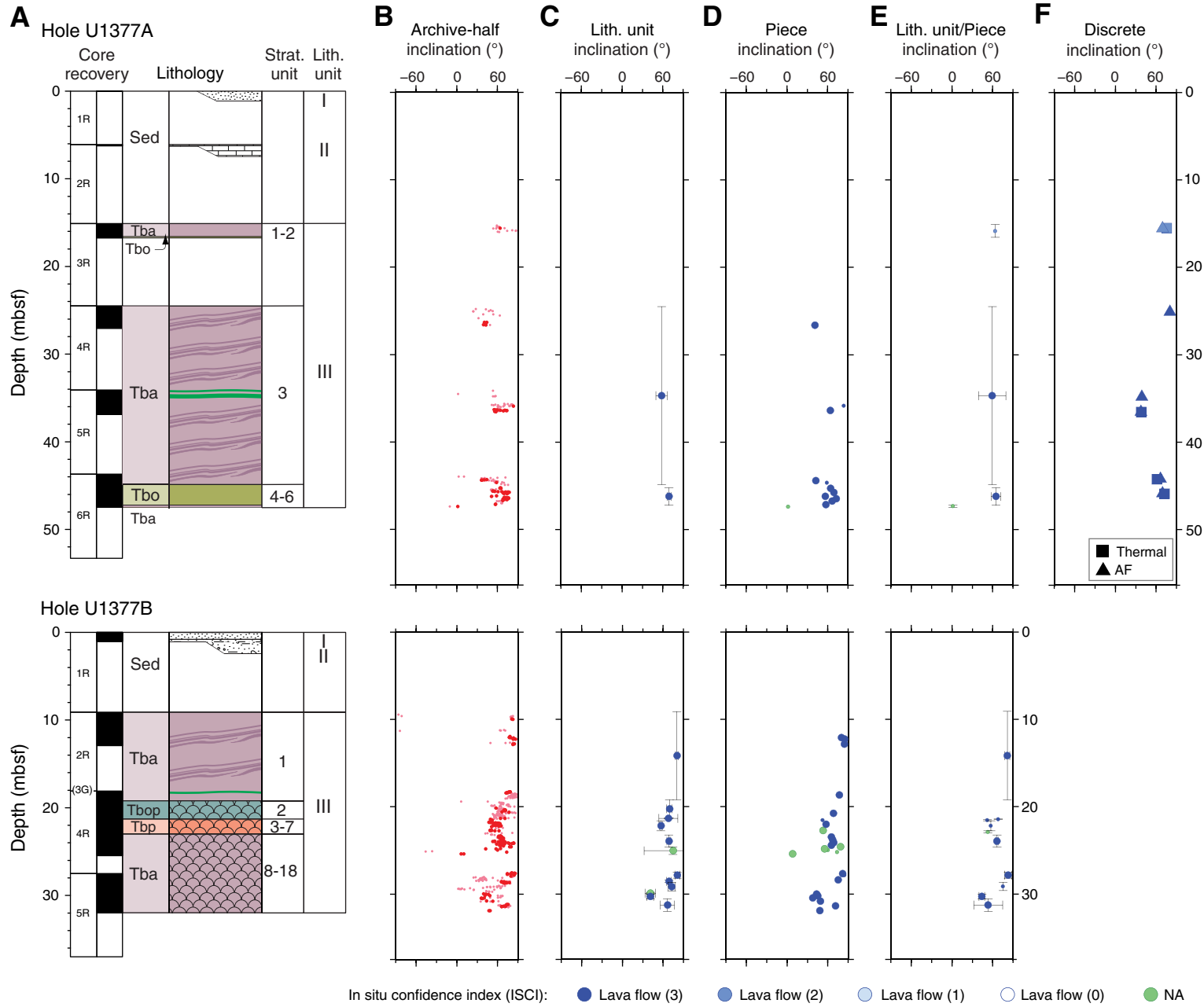


**Figure F31.** Whole-round samples collected for microbiology analysis, Site U1377.



Core, section, interval (cm)	Depth (mbsf)	Lithology	Photograph
330-U1377A-			
6R-3, 56-66	46.84	Moderately olivine-phyric trachybasalt	
330-U1377B-			
4R-1, 0-8	18.10	Aphyric trachybasalt	

Table T1. Coring summary, Site U1377.

Hole U1377A										
Latitude:	38°10.9808'S									
Longitude:	168°38.2620'W									
Water depth (m):	1250.8									
Date started (UTC):	2030 h, 4 February 2011									
Date finished (UTC):	0515 h, 6 February 2011									
Time on hole (days):	1.4									
Seafloor depth DRF (m):	1262.0									
Seafloor depth estimation method:	Tag									
Rig floor to sea level (m):	11.2									
Penetration DSF (m):	53.3									
Cored interval (m):	53.3									
Recovered length (m):	8.76									
Recovery (%):	16									
Drilled interval (m):	NA									
Number of drilled interval:	0									
Total number of cores:	6									
Number of APC cores:	0									
Number of XCB cores:	0									
Number of RCB cores:	6									
Number of other cores:	0									
Hole U1377B										
Latitude:	38°11.2500'S									
Longitude:	168°38.2587'W									
Water depth (m):	1250.8									
Date started (UTC):	0515 h, 6 February 2011									
Date finished (UTC):	1830 h, 7 February 2011									
Time on hole (days):	1.6									
Seafloor depth DRF (m):	1262.0									
Seafloor depth estimation method:	Tag									
Rig floor to sea level (m):	11.2									
Penetration DSF (m):	37.0									
Cored interval (m):	37.0									
Recovered length (m):	14.47									
Recovery (%):	39									
Drilled interval (m):	NA									
Number of drilled interval:	0									
Total number of cores:	5									
Number of APC cores:	0									
Number of XCB cores:	0									
Number of RCB cores:	4									
Number of other cores:	1									
Core	Date (2011)	Time UTC (h)	Depth drilled (m DSF)		Advanced (m)	Recovered length (m)	Curated length (m)	Depth cored (m CSF)		Recovery (%)
			Top	Bottom				Top	Bottom	
330-U1377A-										
1R	5 Feb	0350	0.0	6.1	6.1	0.03	0.03	0.0	0.0	0
2R	5 Feb	0855	6.1	15.1	9.0	0.14	0.14	6.1	6.2	2
3R	5 Feb	1245	15.1	24.5	9.4	1.34	1.65	15.1	16.8	14
4R	5 Feb	1725	24.5	34.1	9.6	1.85	2.56	24.5	27.1	19
5R	5 Feb	2225	34.1	43.7	9.6	2.15	2.79	34.1	36.9	22
6R	6 Feb	0650	43.7	53.3	9.6	3.25	3.76	43.7	47.5	34
330-U1377B-										
1R	6 Feb	1245	0.0	9.1	9.1	1.09	1.08	0.0	1.1	12
2R	6 Feb	1805	9.1	18.1	9.0	2.77	3.82	9.1	12.9	31
3G	6 Feb	2130	0.0	18.1	18.1	2.11	2.11	0.0	2.1	12
4R	7 Feb	0615	18.1	27.5	9.4	6.60	7.37	18.1	25.8	70
5R	7 Feb	1055	27.5	37.0	9.5	4.01	4.48	27.5	32.0	42
Site U1377 totals:					108.4	25.34	29.79			

NA = not applicable. UTC = universal time coordinated. DRF = drilling depth below rig floor, DSF = drilling depth below seafloor, CSF = core depth below seafloor. APC = advanced piston corer (core type H), XCB = extended core barrel (core type X), RCB = rotary core barrel (core type R), G = ghost core.

**Table T2.** Distribution of Cenozoic calcareous nannofossils, Holes U1377A and U1377B.

Core, section interval (cm)	Top depth (mbsf)	Bottom depth (mbsf)	Strat. unit	Zone	Age	Preservation	<i>Calcidiscus leptoporus</i>	<i>Calcidiscus macintyreii</i>	<i>Ceratolithus cristatus</i>	<i>Coccolithus pelagicus</i>	<i>Discoaster brouweri</i>	<i>Discoaster pentaradiatus</i>	<i>Gephyrocapsa</i> sp.	<i>Gephyrocapsa caribbeanica</i>	<i>Gephyrocapsa oceanica</i>	<i>Helicosphaera kamptneri</i>	<i>Pontosphaera multipora</i>	<i>Pseudoemiliania lacunosa</i>	<i>Reticulofenestra pseudoumbilica</i>	<i>Rhabdosphaera clavigera</i>	<i>Armaurolithus primus</i>
330-U1377A-1R-1, 0–3	0.00	0.03	I	CN13–CN15	mid-Pleistocene–Holocene	M	F		F	R			A	F	F	F	F	F	F	F	F
1R-1, 0–3	0.00	0.03	I	CN13–CN15	mid-Pleistocene–Holocene	M	F	R	F	F			A	F	F	F	F	F	F	F	F
330-U1377B-1R-2, 28	1.07	1.07	I	CN13–CN15	mid-Pleistocene?–Holocene	M	F		R	F		R	A	F	F	F	F	F	F	F	R

Preservation: M = moderate. Abundance: A = abundant, F = few, R = rare.

**Table T3.** Distribution of planktonic foraminifers, Hole U1377A.

Core, section interval (cm)	Top depth (mbsf)	Bottom depth (mbsf)	Strat. unit	Zone	Age	Preservation	Group abundance	<i>Globigerina bulloides</i>	<i>Globigerina falconensis</i>	<i>Globigerinoides extremus</i>	<i>Globigerinoides immaturus</i>	<i>Globigerinoides quadrilobatus</i>	<i>Globigerinoides ruber</i>	<i>Globorotalia (Globoconella) inflata</i>	<i>Globorotalia (Hirsutella) scitula</i>	<i>Globorotalia (Truncorotalia) crassaformis</i>	<i>Globorotalia (Truncorotalia) truncatulinoidea</i>	<i>Neoglobobulimina dutertrei</i>	<i>Orbulina universona</i>	<i>Sphaeroidinellopsis seminulina</i>
330-U1377A-1R-1, 0–3	0.00	0.03	I	PL2–PT1b	early Pliocene–Holocene	G	A	F	R	R	P	P	R	A	R	A	R	P	F	P
3R-1, 116–121	16.26	16.31	III	ND	Unidentified		B													
4R-2, 27–30	26.18	26.21	III	ND	Unidentified		B													

ND = not defined. Preservation: G = good. Abundance: A = abundant, F = few, R = rare, P = present, B = barren.



**Table T4.** Distribution of planktonic foraminifers, Hole U1377B.

Core, section interval (cm)	Top depth (mbsf)	Bottom depth (mbsf)	Strat. unit	Zone	Age	Preservation	Group abundance	<i>Globigerina bulloides</i>	<i>Globigerinoides extremus</i>	<i>Globigerinoides trilobus</i>	<i>Globorotalia (Globocornella) inflata</i>	<i>Globorotalia (Truncorotalia) crassaformis</i>	<i>Globorotalia (Truncorotalia) tosaensis</i>	<i>Globorotalia (Truncorotalia) truncatulinoides</i>	<i>Orbulina universa</i>	<i>Sphaeroidinellopsis seminulina</i>
330-U1377B-1R-2, 28–29 2R-3, 20–40	1.07 12.00	1.08 12.20	I III	PL2–PT1b ND	early Pliocene–Holocene Unidentified	G A B	R R P A A	R R P A A	R A R R							

ND = not defined. Preservation: G = good. Abundance: A = abundant, R = rare, P = present, B = barren.

**Table T5.** Distribution of macro- and microfossils observed in thin section, Holes U1377A and U1377B.

Core, section interval (cm)	Top depth (mbsf)	Bottom depth (mbsf)	Strat. unit	Zone	Age	<i>Acarina</i> spp.	<i>Globigerinatheka</i> sp.	<i>Morozovella</i> sp.	<i>Subbotina</i> spp.	Benthic foraminifers	Macrofossils	Planktonic foraminifers
330-U1377A-2R-1W, 15–17	6.25	6.27	II	E8–E16	middle–late Eocene	P	P	P	P	P	B	P
330-U1377B-1R-2W, 8–12	0.87	0.91	II	P4b–E2?	late Paleocene–early Eocene?	P	P	P	P	P	P	P

Abundance: P = present (number of individuals was not counted), B = barren.

**Table T6.** In situ confidence index (ISCI) for igneous lithologic units, Site U1377.

Lith. unit	ISCI	Core, section, interval (cm)	Unit description	Strat. unit
330-U1377A-				
1	2	3R-1, 0, to 3R-1, 148	Massive or lobate flow	III
2	0	3R-2, 0, to 3R-2, 17	Massive or lobate flow	III
3	3	4R-1, 0, to 6R-1, 116	Massive or lobate flow	III
4	1	6R-1, 116, to 6R-2, 15	Massive or lobate flow	III
5	3	6R-2, 15, to 6R-3, 92	Massive or lobate flow	III
6	NA	6R-3, 92, to 6R-3, 118	Rubble	III
330-U1377B-				
1	3	2R-1, 0, to 4R-1, 111	Massive or lobate flow	III
2	3	4R-1, 111, to 4R-3, 122	Pillows	III
3	3	4R-3, 122, to 4R-3, 134	Pillows	III
4	3	4R-3, 134, to 4R-3, 141	Pillows	III
5	3	4R-4, 0, to 4R-4, 12	Pillows	III
6	3	4R-4, 12, to 4R-4, 130	Pillows	III
7	NA	4R-4, 130, to 4R-5, 4	Brecciated base of Unit 6	III
8	NA	4R-5, 4, to 4R-5, 29	Protrusion from Unit 9	III
9	3	4R-5, 29, to 4R-6, 29	Pillows	III
10	NA	4R-6, 29, to 4R-6, 113	Fragmented lava	III
11	3	5R-1, 0, to 5R-1, 69	Pillows	III
12	3	5R-1, 69, to 5R-1, 93	Protrusion between pillows	III
13	3	5R-1, 93, to 5R-1, 117	Pillows	III
14	3	5R-1, 117, to 5R-2, 63	Pillows	III
15	NA	5R-2, 63, to 5R-2, 81	Brecciated interval	III
16	NA	5R-2, 81, to 5R-2, 104	Pillows	III
17	3	5R-2, 104, to 5R-3, 23	Protrusion into Unit 16	III
18	3	5R-3, 23, to 5R-4, 18	Pillows	III

ISCI: 0 = unlikely to be in situ, 1 = could be in situ, 2 = probably in situ, 3 = highly likely to be in situ, NA = not applicable. See “[Igneous petrology and volcanology](#)” in the “Methods” chapter (Expedition 330 Scientists, 2012a) for a full explanation of the ISCI.

Table T7. Whole-rock major and trace element composition, Hole U1377A.

Hole:	330-U1377A-
Core, section:	3R-2
Piece:	1
Interval (cm):	2-4
Top depth (mbsf):	16.6
Strat. unit:	III
Major element oxide (wt%):	
SiO <sub>2</sub>	54.27
TiO <sub>2</sub>	3.80
Al <sub>2</sub> O <sub>3</sub>	18.40
Fe <sub>2</sub> O <sub>3</sub> <sup>T</sup>	6.92
MnO	0.04
MgO	2.96
CaO	6.09
Na <sub>2</sub> O	3.92
K <sub>2</sub> O	1.76
P <sub>2</sub> O <sub>5</sub>	0.51
Total:	98.68
LOI	3.0
Major element oxide (wt%) normalized to 100 wt%:	
SiO <sub>2</sub>	55.00
TiO <sub>2</sub>	3.85
Al <sub>2</sub> O <sub>3</sub>	18.65
Fe <sub>2</sub> O <sub>3</sub> <sup>T</sup>	7.01
MnO	0.04
MgO	3.00
CaO	6.18
Na <sub>2</sub> O	3.97
K <sub>2</sub> O	1.79
P <sub>2</sub> O <sub>5</sub>	0.52
Total:	100.00
Mg#	49.9
Trace element (ppm):	
Ba	240
Sr	566
Zr	280
Y	24
V	281
Sc	29
Cu	95
Zn	28
Co	122
Cr	686
Ni	421

LOI = weight loss on ignition at 930°C. For this sample, the chemical analysis was performed before LOI measurement (see text). Fe<sub>2</sub>O<sub>3</sub><sup>T</sup> = total iron expressed as Fe<sub>2</sub>O<sub>3</sub>. Mg# =  $100 \times \text{Mg}^{2+}/(\text{Mg}^{2+} + \text{Fe}^{2+})$ , assuming that Fe<sub>2</sub>O<sub>3</sub>/FeO = 0.15.



**Table T8.** Moisture and density and compressional wave velocity measurements, Site U1377.

Core, section, interval (cm)	Top depth (mbsf)	Density (g/cm <sup>3</sup> )			Void ratio	Water content (%)	Porosity (%)	Velocity (km/s)			
		Bulk	Dry	Grain				x	y	z	Average
330-U1377A-											
3R-1 44-46	15.54	2.191	1.852	2.770	0.496	15.50	33.16	3.175	3.257	3.217	3.217
4R-1 60-62	25.10	2.434	2.204	2.844	0.291	9.47	22.52	3.678	3.601	3.718	3.666
5R-1 70-72	34.80	2.491	2.244	2.958	0.319	9.93	24.16	3.798	3.649	3.724	3.724
5R-2 94-96	36.53	2.528	2.338	2.871	0.228	7.53	18.58	4.387	4.381	4.388	4.385
6R-1 49-51	44.19	2.507	2.335	2.804	0.201	6.83	16.71	4.310	4.295	4.319	4.308
6R-2 79-81	45.85	2.437	2.170	2.936	0.353	10.95	26.07	3.881	3.941	3.896	3.906
330-U1377B-											
2R-3 99-101	12.79	NA	NA	NA	NA	NA	NA	4.748	4.718	4.637	4.701
4R-1 74-76	18.84	NA	NA	NA	NA	NA	NA	3.252	3.165	3.198	3.205
4R-2 70-72	20.04	NA	NA	NA	NA	NA	NA	4.628	4.791	4.718	4.712
4R-4 91-93	22.39	NA	NA	NA	NA	NA	NA	4.141	4.179	4.149	4.156
4R-6 0-2	24.34	NA	NA	NA	NA	NA	NA	4.462	4.455	4.458	4.458
5R-2 25-27	29.24	NA	NA	NA	NA	NA	NA	3.539	3.532	3.540	3.537
5R-3 56-58	30.87	NA	NA	NA	NA	NA	NA	3.617	3.610	3.631	3.619

Water content is relative to wet mass. Values of compressional wave velocity are accurate to  $\pm 20$  m/s. Moisture and density measurements for Hole U1377B are not available because of time constraints at the end of the expedition (denoted not applicable [NA]).

**Table T9.** Magnetic properties and demagnetization results for discrete samples, Site U1377. This table is available in an [oversized format](#).

**Table T10.** Anisotropy of magnetic susceptibility results for discrete samples, Site U1377. This table is available in an [oversized format](#).



Table T11. Inclination-only averages for lithologic units, Site U1377.

Strat. unit	Lith. unit	ISCI	Lithology	Lith. unit depth (mbsf)		Averages from 2 cm archive-half core data					Averages from Fisher piece averages				
				Top	Bottom	n	Inclination (°)		$\alpha_{63}$	$\alpha_{95}$	n	Inclination (°)		$\alpha_{63}$	$\alpha_{95}$
							Arithmetic mean	Maximum likelihood				Arithmetic mean	Maximum likelihood		
330-U1377A-															
I	—	NA	Sediment	0.00	0.03										
II	—	NA	Sediment	6.10	6.24										
III	1	2	Lava body or intrusive sheet	15.10	16.58	1	63.6				1	63.6			
III	2	0	Lava body	16.58	16.75										
III	3	3	Lava lobes stack or pillow stack	24.50	44.86	21	55.0	58.2	20.3	8.2	6	55.2	59.6	23.4	20.0
III	4	1	Lava lobes stack or pillow stack	44.86	45.21										
III	5	3	Lava lobes stack or pillow stack	45.21	47.20	40	67.7	69.0	10.3	2.9	6	64.2	64.8	8.5	7.1
III	6	NA	Lava lobes stack or pillow stack	47.20	47.46	1	1.4				1	1.4			
330-U1377B-															
I	—	NA	Sediment	0.00	0.79										
II	—	NA	Sediment	0.79	1.08										
III	1	3	Lava lobes or pillows	9.10	19.21	21	79.3	80.2	5.7	2.2	6	80.8	81.4	4.3	3.6
III	2	3	Lava lobes or pillows	19.21	21.29	11	68.6	69.2	7.4	4.2					
III	3	3	Pillows	21.29	21.41	2	67.4	67.6	4.5	13.8					
III	4	3	Pillows	21.41	21.48	1	49.3				1	68.1			
III	5	3	Pillows	21.48	21.60	1	52.1				1	52.1			
III	6	3	Lava lobes or pillows	21.60	22.78	30	56.2	56.6	7.6	2.5	1	57.3			
III	7	NA	Brecciated base of Unit 6	22.78	22.99	1	61.9				1	52.9			
III	8	NA	Possible break out of Unit 9?	22.99	23.24										
III	9	3	Lava lobes or pillows	23.24	24.63	42	67.2	68.3	10.0	2.8	4	66.4	66.4	2.0	2.3
III	10	NA	Fragmented lava	24.63	25.47	7	44.8	74.4	48.0	42.3	5*				
III	11	3	Pillows	27.50	28.19	11	79.7	80.7	6.0	3.4	2	82.8	82.9	1.7	5.3
III	12	3	Intrusive lava in interpillow voids (break out)	28.19	28.43										
III	13	3	Pillows	28.43	28.67	5	68.4	68.6	3.7	3.5					
III	14	3	Pillows	28.67	29.62	4	72.2	72.5	4.7	5.3	1	75.2			
III	15	NA	Brecciated interval	29.62	29.80										
III	16	NA	Pillows	29.80	30.03	2	41.2	41.2	2.5	7.9					
III	17	3	Lava body with glassy margin, seems intrusive into Unit 16	30.03	30.54	7	40.9	41.1	6.5	4.9	2	44.1	44.1	1.3	4.1
III	18	3	Pillows	30.54	31.98	11	62.4	66.1	18.0	10.4	4	51.4	53.4	18.1	21.0

\* = no solution possible. — = no lithologic unit. ISCI = in situ confidence index (see “Igneous petrology and volcanology” in the “Methods” chapter [Expedition 330 Scientists, 2012a]). NA = not applicable. The method of Arason and Levi (2010) was used to calculate inclination-only mean and associated statistics.  $\alpha_{63}$  = circular standard deviation,  $\alpha_{95}$  = 95% confidence angle.

**Table T12.** Culturing efforts, Hole U1377B.

Core, section, interval (cm)	Media	Vials inoculated (N)	Growth
330-U1377B-4R-1, 0-8	Autotrophic S oxidizers	2	ND
	Heterotrophic S oxidizers	2	ND
	Autotrophic Fe reducers	2	ND
	Heterotrophic Fe reducers	2	ND
	Autotrophic Fe oxidizers	2	ND
	Heterotrophs; 1% marine broth (low oxygen)	2	ND
	Heterotrophs; 10% marine broth (low oxygen)	2	ND
	Heterotrophs; 1% marine broth (saturated oxygen)	2	ND
	Heterotrophs; 10% marine broth (saturated oxygen)	2	ND

Analysis of growth was not determined (ND) because incubations had to be packed for postexpedition shipping.

**Table T13.** Samples used for stable isotope addition bioassays, Site U1377.

Core, section, interval (cm)	Treatment	Vials (N)	Approximate volume of rocks per vial (cm <sup>3</sup> )
330-U1377A-6R-3, 56-66	+2.71 mM <sup>13</sup> C bicarbonate +300 μM <sup>34</sup> S elemental S +0.5 μM <sup>15</sup> N ammonia	5	23
	+2.71 mM <sup>13</sup> C bicarbonate +300 μM <sup>34</sup> S elemental S +0.5 μM <sup>15</sup> N ammonia	2 (dead)	23
330-U1377B-4R-1, 0-8	+2.71 mM <sup>13</sup> C bicarbonate +300 μM <sup>34</sup> S elemental S +0.5 μM <sup>15</sup> N ammonia	5	23
	+2.71 mM <sup>13</sup> C bicarbonate +300 μM <sup>34</sup> S elemental S +0.5 μM <sup>15</sup> N ammonia	1 (dead)	23